IC 9294

BUREAU OF MINES
INFORMATION CIRCULAR/1991

Hydraulic Borehole Pressure Cells: Equipment, Technique, and Theories

By Khamis Y. Haramy and R. O. Kneisley

UNITED STATES DEPARTMENT OF THE INTERIOR

Mission: As the Nation's principal conservation agency, the Department of the Interior has responsibility for most of our nationally-owned public lands and natural and cultural resources. This includes fostering wise use of our land and water resources, protecting our fish and wildlife, preserving the environmental and cultural values of our national parks and historical places, and providing for the enjoyment of life through outdoor recreation. The Department assesses our energy and mineral resources and works to assure that their development is in the best interests of all our people. The Department also promotes the goals of the Take Pride in America campaign by encouraging stewardship and citizen responsibility for the public lands and promoting citizen participation in their care. The Department also has a major responsibility for American Indian reservation communities and for people who live in Island Territories under U.S. Administration.

Information Circular 9294

Hydraulic Borehole Pressure Cells: Equipment, Technique, and Theories

By Khamis Y. Haramy and R. O. Kneisley

UNITED STATES DEPARTMENT OF THE INTERIOR
Manuel Lujan, Jr., Secretary

BUREAU OF MINES
T S Ary, Director

Library of Congress Cataloging in Publication Data:

Haramy, Khamis Y.

Hydraulic borehole pressure cells : equipment, technique, and theories / by Khamis Y. Haramy and R.O. Kneisley.

p. cm. — (Information circular; 9294)

Includes bibliographical references (p. 23).

Supt. of Docs. no.: I 28.27:9294.

1. Ground control (Mining). 2. Rock pressure—Measurement. 3. Pressure gages. I. Kneisley, R. O. (Richard O.) II. Title. III. Series: Information circular (United States. Bureau of Mines); 9294.

TN295.U4 [TN288] 622 s—dc20 [622' .28] 91-10789 CIP

CONTENTS

ILLUSTRATIONS

UNIT OF MEASURE ABBREVIATIONS USED IN THIS REPORT

ft	foot	lb/in^3	pound per cubic inch
GPa	gigapascal	MPa	megapascal
in	inch	psi	pound per square inch
in^3	cubic inch	psi-ft	pound per square inch-foot
in^{-4}/lb	1 over inch to the fourth power per pound		

HYDRAULIC BOREHOLE PRESSURE CELLS: EQUIPMENT, TECHNIQUE, AND THEORIES

By Khamis Y. Haramy[1] and R. O. Kneisley[2]

ABSTRACT

This U.S. Bureau of Mines report describes the use of Bureau-developed flat and cylindrical hydraulic borehole pressure cells. A brief description of the fabrication, installation, and pressurizing equipment is given, and pressurizing procedures are discussed. Theories available on evaluation of data from the flat and cylindrical pressure cells and examples of data analysis and stress evaluation are also presented.

[1]Supervisory mining engineer.
[2]Mining engineer.
Denver Research Center, U.S. Bureau of Mines, Denver, CO.

INTRODUCTION

The flat and cylindrical borehole pressure cells were developed by the U.S. Bureau of Mines in the late 1950's (*1*)[3] as part of the Bureau's long-range ground control program to improve miners' safety. The cells are used to measure mining-induced pressure changes in the mine structure. A brief description of the pressure cell method is as follows: Boreholes are drilled into the mine structure, and pressure cells are installed in each borehole and pressurized to contact the surface of the hole. As the hole deforms under changing stress conditions, the deformation is converted to pressure changes through hydraulic fluid in the pressure cells. The pressure changes are monitored with gauges or continuous mechanical chart recorders, or converted to an electrical signal by transducers and read using data loggers. Although different types of hydraulic pressure cells are available, this report discusses the types developed and used at the Bureau's Denver Research Center.

The hydraulic pressure cells have several uses, such as the determination of premining and mining-induced pressures and/or pressure changes, and the determination of in situ physical properties of rock mass. This report briefly describes the flat and cylindrical borehole pressure cells and summarizes methods available for data analysis. No preference is given to any of the methods.

EQUIPMENT AND TECHNIQUE

CYLINDRICAL BOREHOLE PRESSURE CELL

The cylindrical borehole pressure cell (CPC) measures radial pressure changes in the rock and does not distinguish between horizontal and vertical pressure changes. The CPC consists of a copper shell brazed to a cylindrical steel core. These two components are shown in figure 1. Glycerine or hydraulic oil is pumped into the annulus between the shell and core and expanded against the borehole wall. The cell diameter is 1.49 in, and the cell is designed to be installed in a 1.5-in-diameter drill hole. The assembled cell is 8 in long, with an effective length of approximately 7 in. Figure 2 shows the CPC connected to the pressurizing and recording equipment.

FLAT BOREHOLE PRESSURE CELL

The flat borehole pressure cell (BPC) measures directional pressure changes, the direction being dependent on the cell orientation. The BPC consists of a flat steel bladder, encapsulated in a 2.34-in-diameter by 8.75-in-long concrete (grout) cylinder, as shown in figure 3. The steel bladder is 2 in wide by 8 in long by 0.35 in thick. During fabrication, two longitudinal holes (tunnels) are normally cast in the concrete jacket (fig. 4). These 1/2-in-OD tunnels run the length of the cell, permitting the passage of hydraulic lines and the installation of several cells in a single borehole. Figure 5 shows a BPC, the installation tool, and the pressurizing and recording equipment. The concrete ratio is a 2-to-1 sand-to-cement mix. For the concrete to gain full strength, each cell is cured for approximately 30 days.

PRESSURIZING SYSTEM

Pressure cells are filled with hydraulic fluid and connected by 1/4-in-OD stainless steel tubing to individual pressure gauges or to continuous chart pressure recorders,

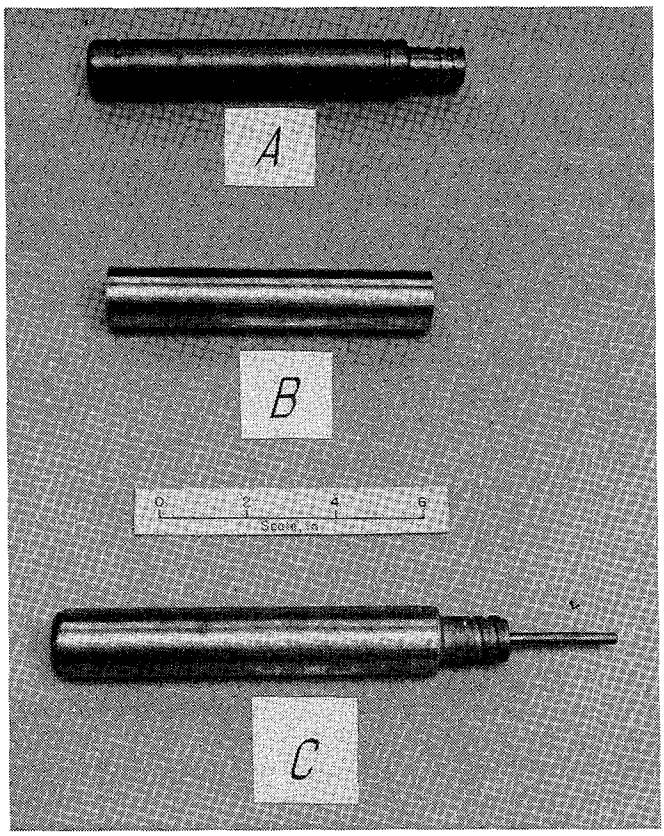

Figure 1.—CPC and components: *A*, inner shell; *B*, expandable outer copper shell; *C*, completely assembled CPC.

[3]Italic numbers in parentheses refer to items in the list of references preceding the appendix.

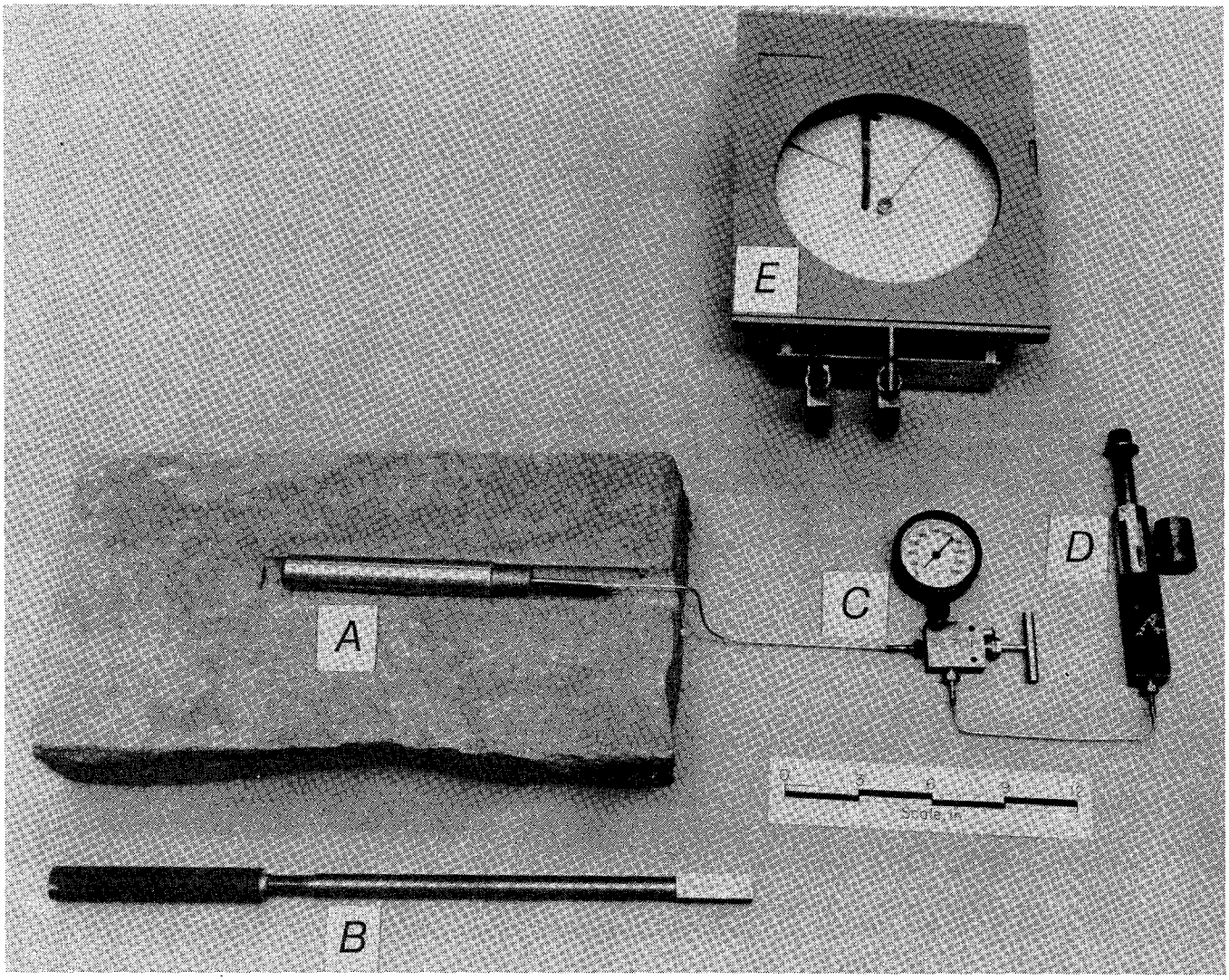

Figure 2.—CPC connected to pressurizing and recording equipment. CPC (*A*) is connected to valve gauge (*C*) and PCM (*D*). Optional mechanical chart recorder (*E*) provides continuous data recording. Component *B* is a section of installation rod.

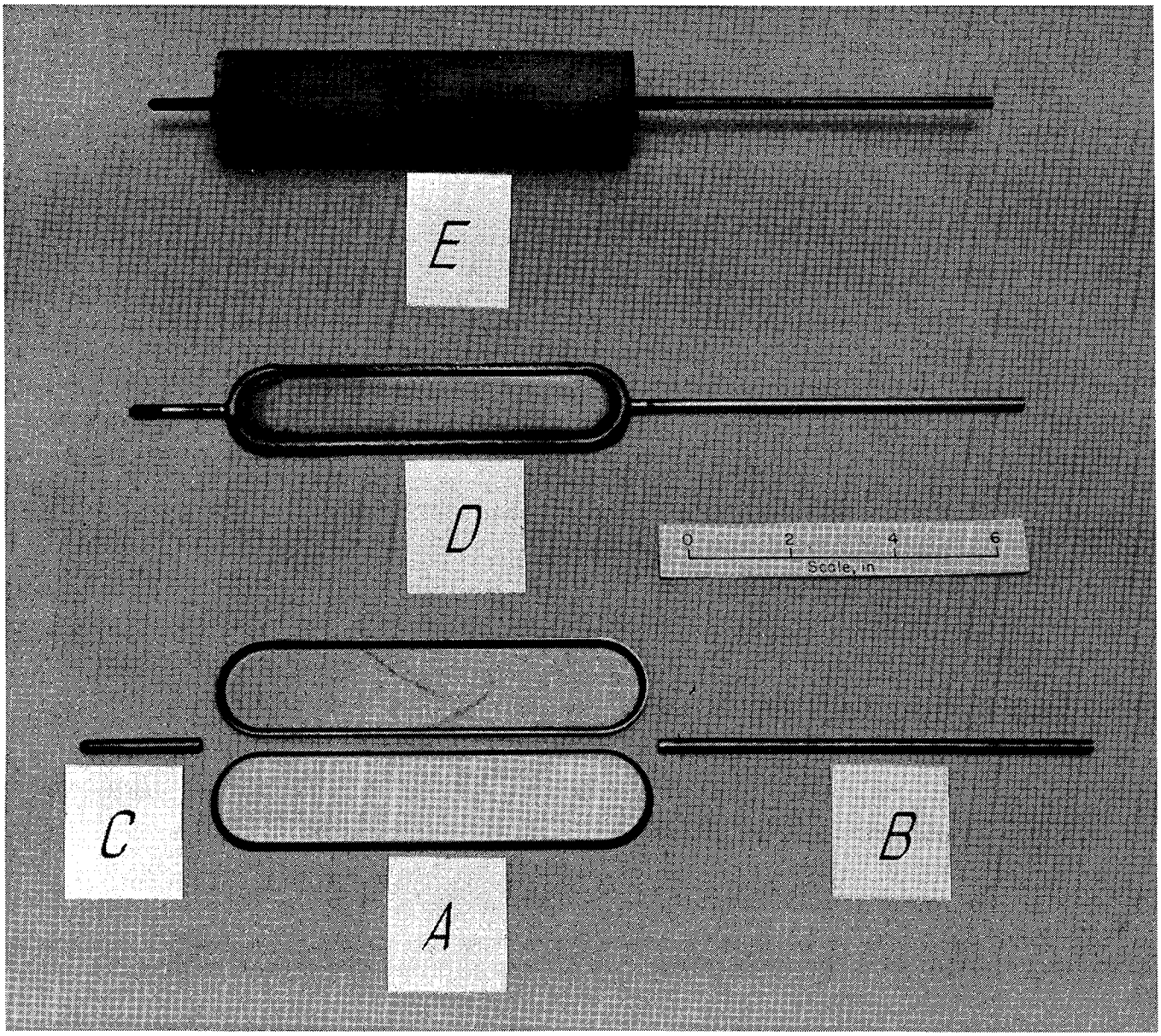

Figure 3.—BPC and components: steel platens (*A*) form completed flatjack (*D*), parts *B* and *C* are stainless steel tubing used to pressurize the BPC, and *E* is the grout-encapsulated BPC.

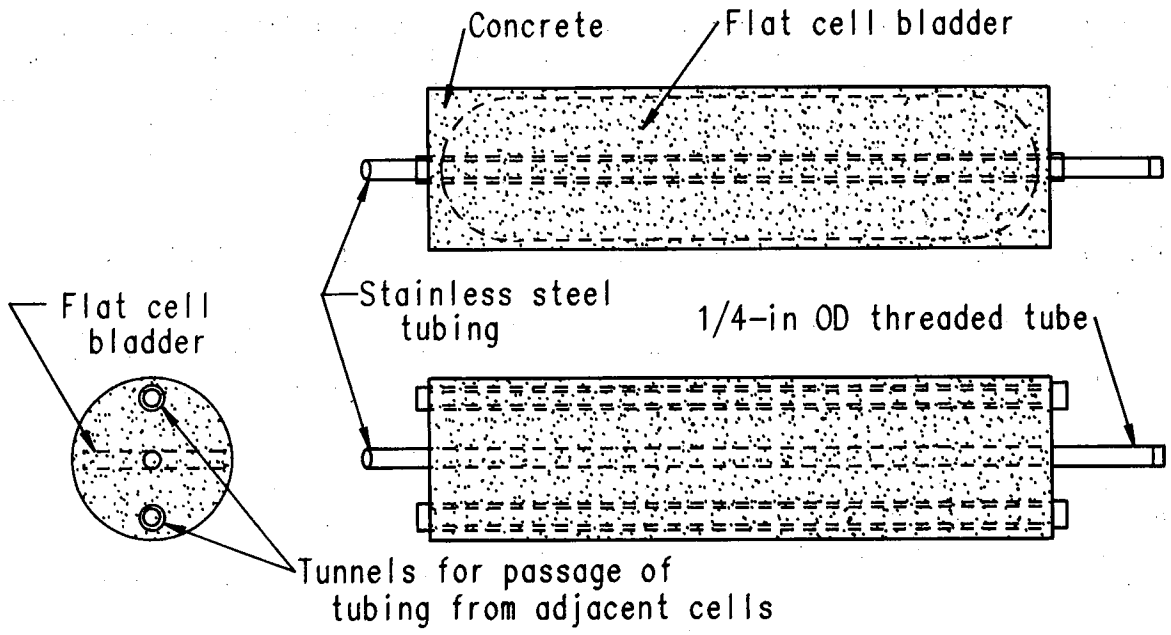

Figure 4.—BPC schematic.

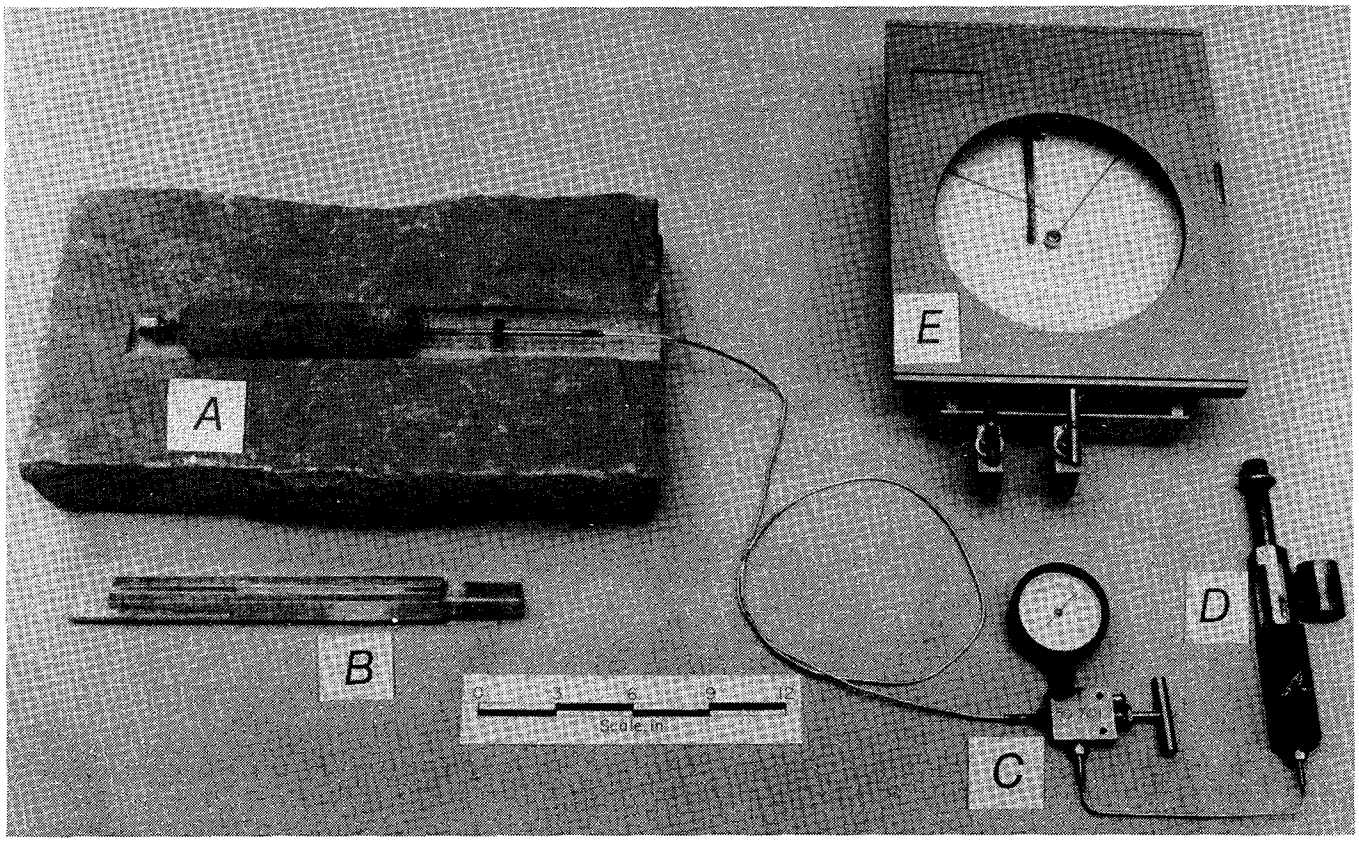

Figure 5.—BPC connected to pressurizing and recording equipment: *A*, BPC; *B*, installation rod; *C*, valve gauge; *D*, PCM; *E*, chart recorder.

as shown in figures 2 and 5. Once the cell is installed at the proper hole depth and in the proper orientation, it is pressurized by means of a pressure control meter (PCM). The PCM (figs. 2, 5) utilizes a threaded piston that measures the volume of the fluid injected into the cell. A detailed schematic of the PCM, patented by Panek (*2*), is shown in figure 6. When pressurized, the cell expands against the concrete jacket, which in turn expands and bears against the borehole walls.

Generally, the initial cell seating pressure is dependent on overburden depth. For example, in an approximately 1,800-ft-deep mine, the cells are set at 2,000 psi (1.1 × depth). Before the cell is pressurized, the hydraulic system should be bled and drained of any air bubbles. As the cell is pressurized, the number of turns on the PCM should be recorded. The number of turns provides a measure of the volume of hydraulic fluid in the system, which in turn provides information on the accuracy of the hole size. Too much fluid (>75 turns) can mean that the hole is significantly larger than the cell. As a result, the pressure cell readings will be less accurate. If the pressure drops slowly immediately after the cell has been pressurized, a leak in the system or a ruptured cell is indicated, although a ruptured cell is rare. Laboratory tests have shown that most of the cells can withstand pressures of up to 20,000 psi.

DRILLING EQUIPMENT

Since a precision hole is required for proper pressure cell installation, special drilling equipment is required. The Bureau uses a post-mounted, air-powered drill, commonly used in underground core drilling operations. The drill, used in conjunction with a precision bit by experienced drillers, provides a precisely drilled hole that permits accurate pressure cell response to changing ground pressures.

A specially designed bit that combines a diamond and a drag bit rapidly drills smooth and precise-diameter instrumentation holes (*3*) (fig. 7).

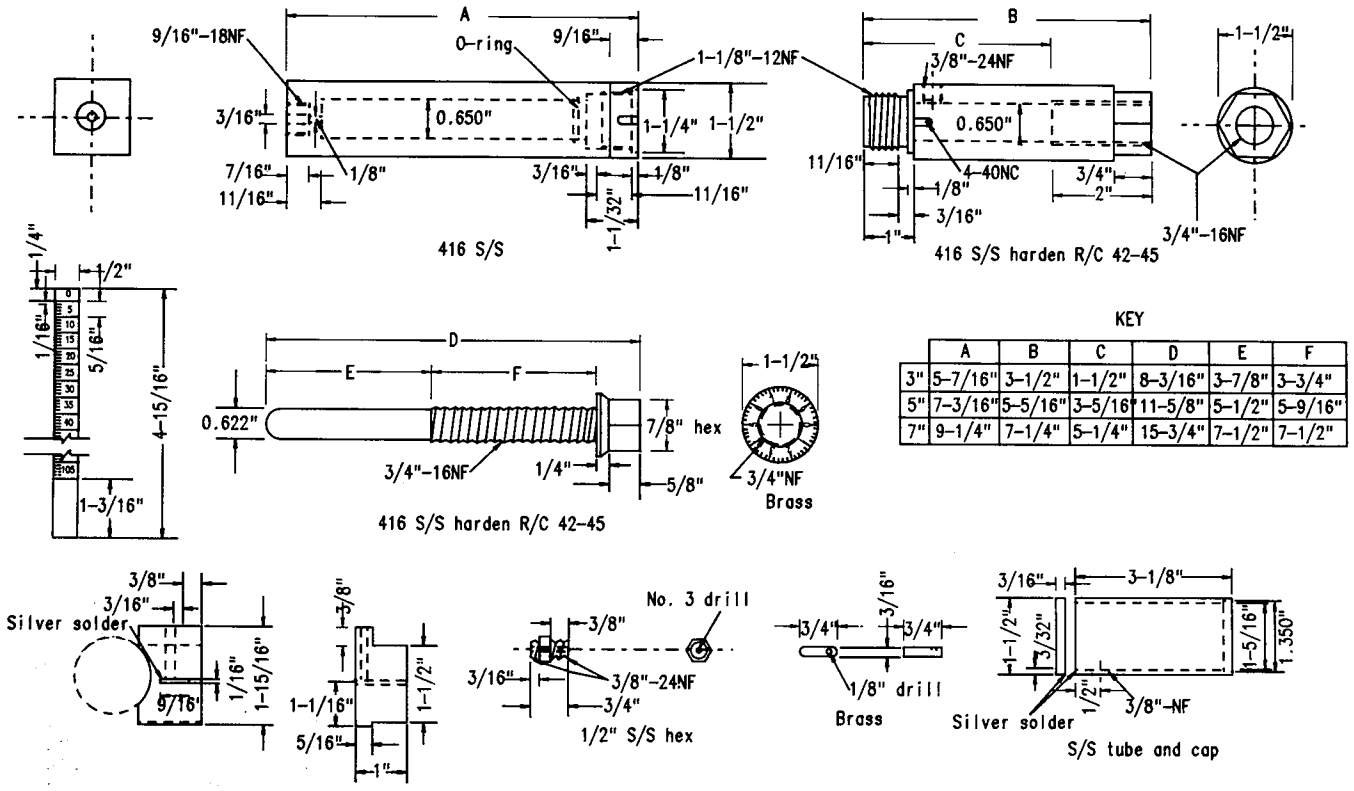

Figure 6.—Detailed schematic of PCM; S/S and R/C are stainless steel and Rockwell hardness number, respectively. [Full-size (18- by 30-in) drawing available from K. Y. Haramy or R. O. Kneisley, Denver Research Center.]

INSTALLATION INSTRUCTIONS

Installation rods are made in 5-ft-long sections of 1-1/4-in-square aluminum tubing. The placement heads, one each for the BPC and CPC, fit onto the installation rods. Detailed drawings of the installation rods and placement heads are contained in figures 8, 9, and 10.

As a cell is installed, the "feel" of the cell is essential. If the hole is squeezed, the cell might not fit through the tight or squeezed spot. Often, a cell can be pushed through a tight spot; however, sometimes redrilling (reaming) the hole may be necessary. If too much pushing force is used, the pressure cell may get stuck in the hole, possibly at an undesirable location and at an incorrect orientation.

It is important not to disconnect the installation rod until the cell is seated and pressurized. Otherwise, the cell may move or rotate, and the orientation will be incorrect. To install more than one cell in a hole requires special attention. Tubing attached to the deepest cell must pass through the tunnels of all cells, as shown in figure 11. This procedure is repeated for the next deepest cell and so on until the shallowest cell is installed.

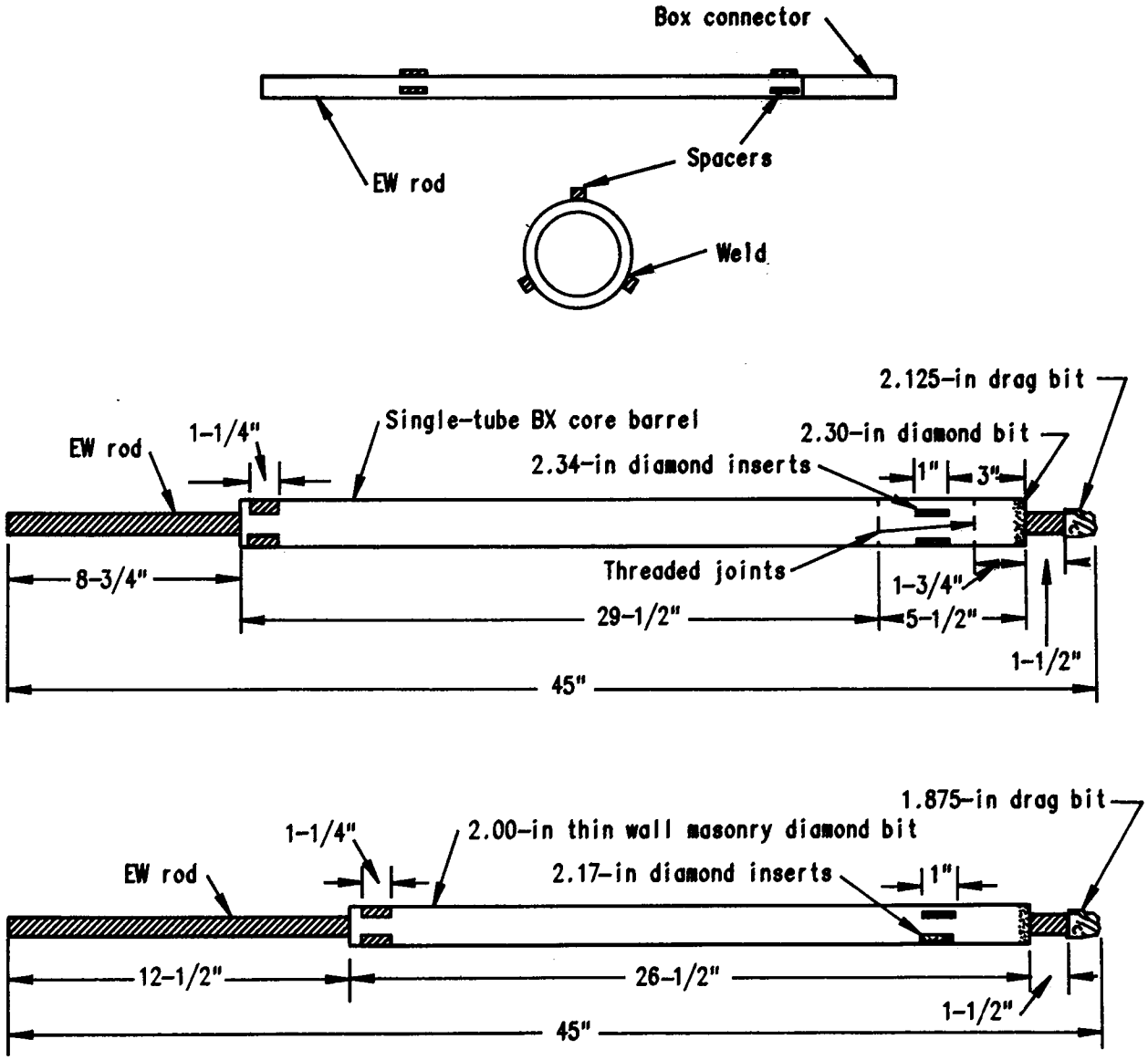

Figure 7.—Combination precision bits.

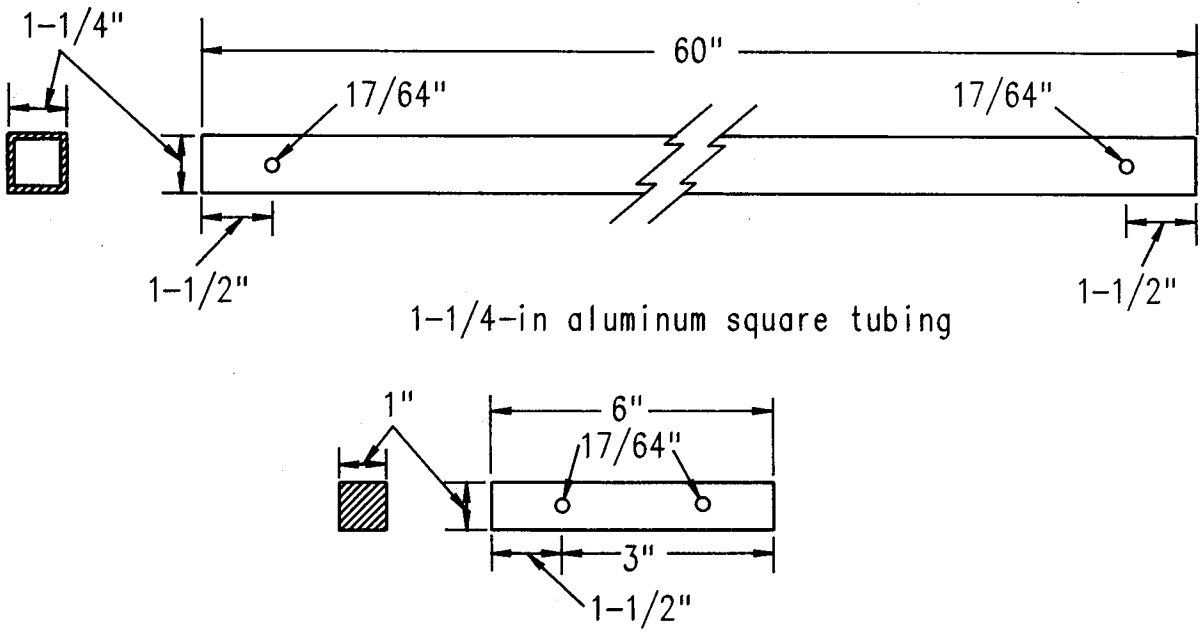

Figure 8.—Pressure cell installation rod.

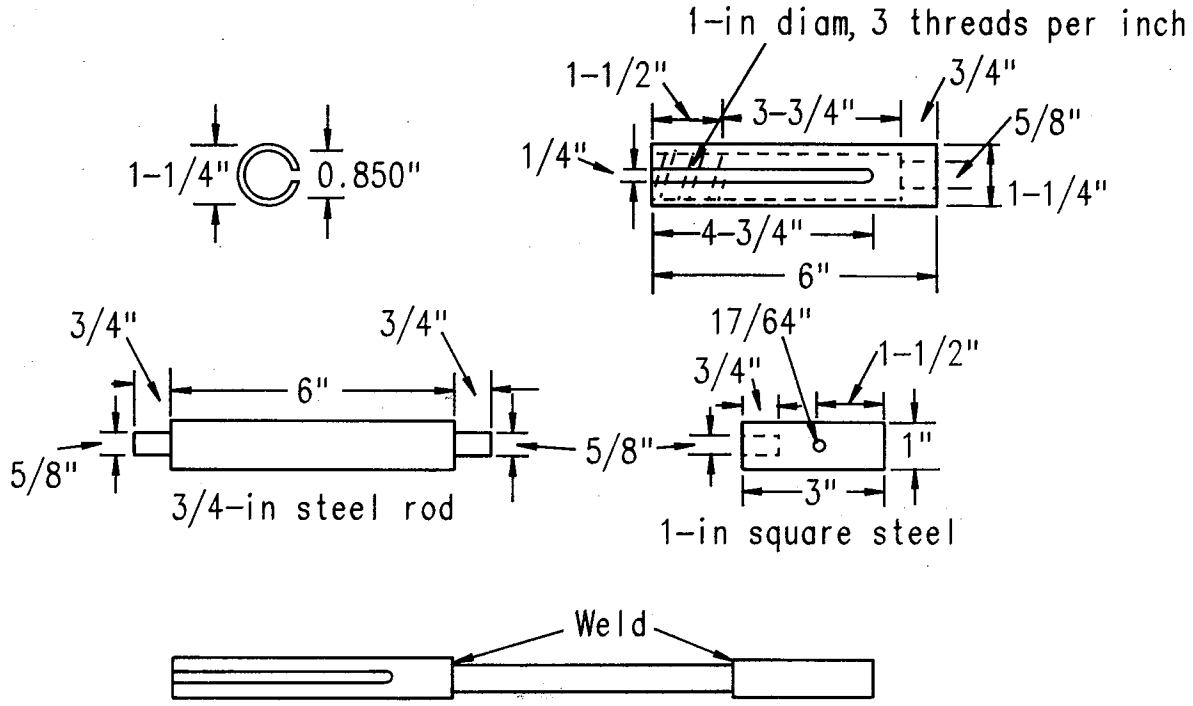

Figure 9.—CPC installation rod head.

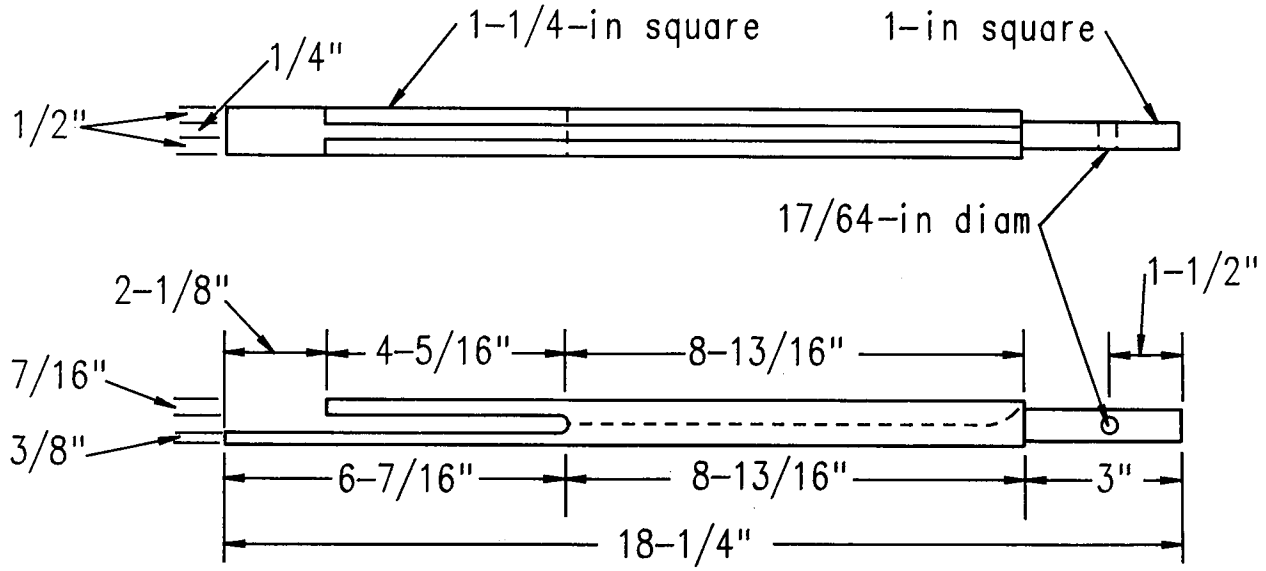

Figure 10.—BPC installation rod head.

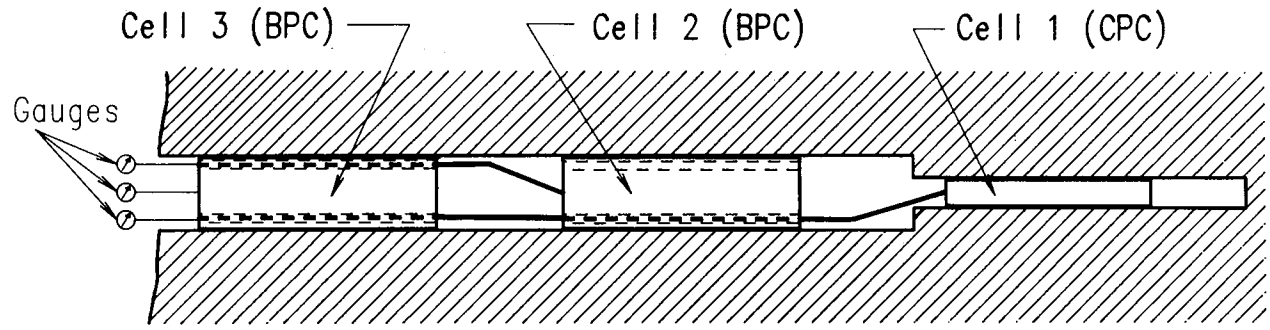

Figure 11.—Schematic of three-cell installation.

PRESSURE CELL DATA ANALYSIS

ROCK STRESS ANALYSIS FROM CELL DATA

This section includes a discussion of the importance of stress measurements; a very brief summary of stress measurement studies; and descriptions, with examples, of techniques available for converting pressure cell measurements to either ground stress and/or changes in ground stress.

Importance of Stress Measurements

Panek (*1-2, 4*) suggests that ground control consists of exercising control of rock displacement or deformation that depends on

- Mine structure—opening and pillar geometries, geologic bedding and jointing,
- Mechanical properties—strengths, elastic properties, and flow characteristics,
- Load duration—time interval that an opening or support structure is exposed to load, and
- Load or applied stress—overburden weight, tectonic stresses, and mining-induced load redistributions.

Control of rock stress is the most complex of the four factors because rock stress is invisible, difficult to measure, and limited to the mining-created rock structure. Stress measurement, whether qualitatively by visual observation

or quantitatively using instrumentation, is essential but very difficult because of rock-instrumentation interaction. While "go"-"no go" gauges may provide data for assessing a given design, they are often of little use for solving particular problems (*1*).

Although displacement is easier to measure, incorrect inferences of stress magnitude and direction can result from measured displacement. Two- and three-dimensional stress analyses reveal that such inferences can lead to erroneous conclusions (*1*). Since rock deformation depends on both pressure and mechanical properties, variations of rock properties within a mine can obscure pressure effects. Since rock deformation also depends in part on load duration, stress measurement may provide an advance warning of ground control problems and provide a basis for corrective action (*1*).

Stress Measurement Studies

Quantitative rock pressure measurements not only provide a means for solving site-specific ground control problems, but also permit comparison between in-mine measurements and more theoretical analyses. Since the early 1960's, the Bureau has been involved in the development and analysis of in situ stress measurement instrumentation and techniques (*5-7*). Early field studies employed borehole pressure cells to monitor stress changes during pillaring, especially under bump-prone conditions (*8*). While such studies were not strictly quantitative (i.e., measured pressure cell readings were not related to actual ground stress), these in-mine investigations proved very useful in relating pressure cell measurements to observed strata behavior. From one such study, Curth (*9*) developed the following relation between pillar pressure and pillar extraction:

$$\Delta P_v = -0.11 A_x + 0.356 A_x^2, \quad (1)$$

where ΔP_v = mean vertical pillar pressure increase,

and A_x = percentage of pillar mined.

The 1970's saw expanded use of hydraulic pressure cells, especially with increased use of mechanized longwalls in the United States. One study included analyses of chain pillar and panel entry performance. Site-specific findings included determination of pressure arch width over longwall panel entries, determination of forward abutment magnitude and extent, and identification of the initial cave and the loading histories of chain pillars and starting room-bleeder entry pillars (*10-11*). A ground control study of shortwall mining used borehole pressure cells to monitor pillar pressure changes and to determine forward abutment extent. Small increases in chain pillar pressure were attributed to the fact that overlying limestone beds did not bridge the panel (*12*).

More recent Bureau studies, while not universally using hydraulic pressure cells, have emphasized some type of pressure and/or pressure change measurements to characterize longwall entry performance (*13-15*), to investigate multiseam interaction in both coal and noncoal deposits (*16-19*), to evaluate mining methods in bump-prone conditions (*20-22*), and to provide in-mine validation of computer-generated analyses (*23-25*). A brief discussion of some western U.S. coal mine studies follows.

Lu (*13*) utilized pressure cells to determine premining ground pressures, to analyze forward abutments, and to investigate load transfer and the residual strength of chain pillars. Results indicated that while vertical stress generally agreed with overburden loading, horizontal stresses usually exceeded the value expected from Poisson's effect. Continuous recording of forward abutment pressure indicated that mining-induced increases extend from 0.23 to 0.33 times the depth ahead of mining, that significant pressure increases begin when the face is approximately 50 ft away, and that a yield zone of width equivalent to about one extraction height exists at the face. Lu suggests that forward abutment magnitude and extent provide a criterion for entry support design. For that portion of the entry subjected to forward abutment pressure, entry support density should be increased in proportion to the increase in abutment pressure.

Haramy (*21*) included analysis of pressure data to describe a possible failure mechanism of a major bump in a deep, western U.S. longwall operation. Abutment pressures were found to consist of two components: a gradual increase associated with main roof load transfer onto the panel and dynamic load increases following bumps. Pressure cells installed in tailgate-side pack walls indicated that pack wall response to a major bump resulted from floor failure. Pressure cell data, combined with longwall shield loading and displacement measurements, indicated that when critical pressures, in part due to an overhanging roof, were reached, the floor failed violently, reducing confinement of the panel rib and bearing strength of the pack wall-floor structural component.

DeMarco (*15*) included analysis from pressure cells installed in chain pillars and longwall panels at a deep, western U.S. longwall mine that used both two- and three-entry systems. Analysis indicated that, from a ground control viewpoint, the two-entry design better met the goals of reduced roof falls, reduced total ground stress, and elimination of concentrated load transfer into future mining areas. Two-entry ground control improvements included reduced areal loading that resulted in fewer roof falls in a zone of more geologically disturbed roof. Lower

stress magnitudes and more evenly distributed loading of the two-entry system suggest improved mining conditions in the lower seam and a reduction of stress concentrations along sand channels, faults, and fracture sets encountered during development.

Hackett (*19*) combined measurements from borehole pressure cells installed under a longwall panel and in the panel to characterize the forward abutment and gob reloading in a Wyoming trona mine. Mining-induced pressure increases began when the face was approximately 0.25 times the depth away, and contrary to most coal mine measurements, no yield zone was observed near the face. Pressure cells installed under the panel indicated that gob reloading stabilized when the face was about 500 ft, or 0.29 times the overburden depth, inby the face.

Kripakov (*16*) included a comparison between computer-generated and in-mine behavior to design mine structures. Computer-generated behavior, based on a combination of finite-element and displacement-discontinuity modeling, was compared with in-mine measurements at five face positions simulating the mining of two adjacent longwall panels. Results indicated qualitative agreement between predicted and observed behavior. Discrepancies were attributed to assumptions of linear elastic behavior that does not simulate fracturing; unrealistically high vertical stress near the pillar edge due, in some extent, to confinement generated by the elastic model; the assumed yield criteria; and in situ physical property values. Regardless of the quantitative differences, the modeled and in-mine results agreed regarding trends of increasing pillar core stress and rib yielding.

Conversion of Cell Readings to Actual Stresses

While the above studies have proven useful, most, if not all, have not included conversion of pressure cell readings to actual rock stresses. Such conversion may be helpful to (1) develop confidence in numerical modeling techniques by providing quantitative comparison between predicted and observed in-mine behavior and (2) validate more theoretical analyses of stress-related, especially three-dimensional, problems. Several investigators have developed methods to determine rock stress and/or rock stress changes from in situ pressure measurements. Following are descriptions of some published techniques for Bureau-developed hydraulic pressure cells. No conclusions are drawn as to which, if any, technique is best or indeed valid; theoretical considerations and mathematical derivations have been minimized but are referenced for further reading, and where possible, examples have been included.

Morgan (*26*) described a method to determine rock stress based on the principle of static equilibrium. This technique utilizes mathematical relationships independent of both elastic properties and stress distribution near the opening. Before mining, a vertical stress, $\sigma_y = \sigma_i$, exists; the premining load on the plane through 0-x (fig. 12) is

$$\int_0^d \sigma_y dx = \int_0^d \sigma_i dx = \sigma_i d, \qquad (2)$$

where d = distance.

Static equilibrium requires that the total load remain constant; the load originally on the opening, $\sigma_i w$, is superimposed on the ribs. Denoting the areas under the stress distributions curves by A_1, A_2, A_3, and A_4, from figure 12*B*, it follows that (*26*)

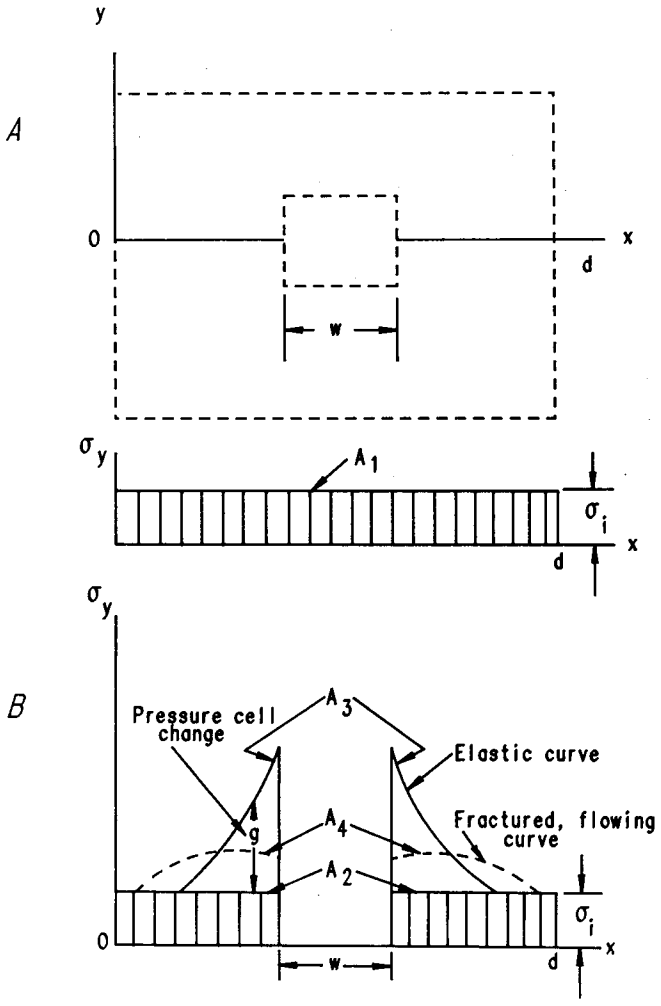

Figure 12.—Illustration of principle of static equilibrium for single opening (*26*). *A*, Single opening of width w through slice O-d; *B*, several possible stress redistributions resulting from driving opening w.

$$A_1 = A_2 + \sigma_i w$$

and $$A_1 = A_3 = A_4,$$

from which $$(A_3 - A_2) = (A_4 - A_2) = \sigma_i w, \quad (3)$$

where A_1, A_2, A_3, A_4 = areas, integrals, of respective stress-distance curves,

w = opening width,

and σ_i = initial vertical stress.

Initial vertical stress, σ_i, is determined graphically from the measured pressure change curve, g, to find the area $(A_3 - A_2)$. Using the opening width, w, and equation 3, the initial stress and the absolute stress, $\sigma_i + g$, can be calculated. No assumptions regarding the actual stress distribution or rock properties (elasticity, isotropy, or homogeneity) are required. It is, however, assumed that the resulting stress redistribution is symmetrical, and that measurements need only be made in one rib (*26*).

Two potential applications of this method follow.

Pressure cells are installed in boreholes from an existing entry (entry A), and initial cell readings are recorded (fig. 13). After the new entry (entry B) is mined, pressure readings are retaken, and the stress change-distance is integrated. Initial stress, σ_i, is calculated using equation 3; the absolute stress is determined by adding the pressure changes to the initial stress, $\sigma_i + g$. Example 1 illustrates use of this technique:

EXAMPLE 1: This example illustrates the use of Morgan's method to determine absolute ground stress from cell data (*26*).

1. Following development of entry A (fig. 13), install pressure cells and record initial readings.

2. Determine area under pressure-distance curve after development of entry A (fig. 14*A*):

Zone	Pressure, zone ends, psi	Average pressure, psi	Zone width, ft	Zone area, psi-ft
1 ...	200, 400	300	12	3,600
2 ...	400, 300	350	16	5,600
3 ...	300, 700	500	16	8,000
4 ...	700, 500	600	12	7,200
5 ...	500, 300	400	16	6,400
Total				30,800

3. Following development of entry B (fig. 13), record and plot cell readings as shown in figure 14*B*.

4. Determine area under pressure-distance curve after development of entry B:

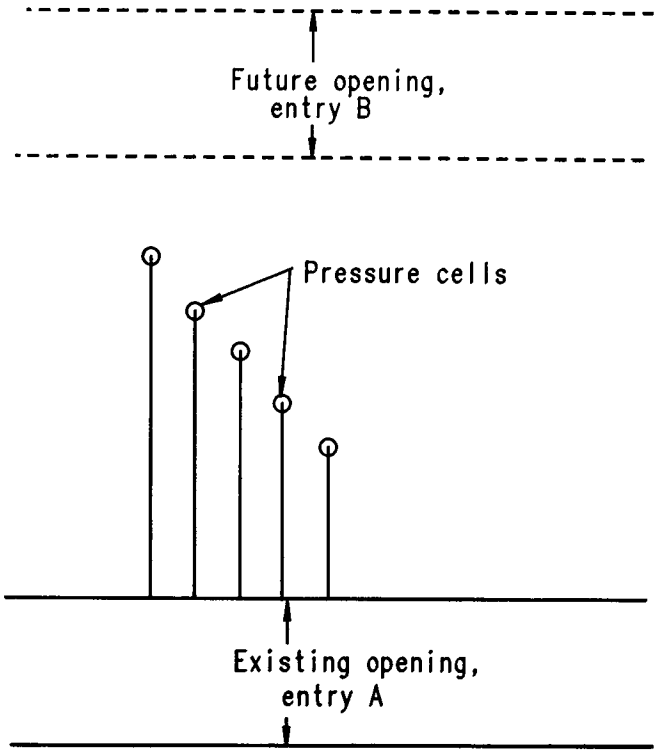

Figure 13.—Determination of σ_i and distribution of σ_y caused by mining new opening (*26*).

Zone	Pressure, zone ends, psi	Average pressure, psi	Zone width, ft	Zone area, psi-ft
1 ...	700, 700	700	12	8,400
2 ...	700, 500	600	16	9,600
3 ...	500, 800	650	16	10,400
4 ...	800, 600	700	12	8,400
5 ...	600, 300	450	16	7,200
Total				44,000

5. Determine initial stress (σ_i):

$$\sigma_i = \frac{A_2 - A_1}{w} = \frac{(44{,}000 - 30{,}800)\ \text{psi-ft}}{32\ \text{ft}} = 412\ \text{psi}.$$

6. Determine absolute stress $(\sigma_i + g)$:

Cell	Pressure, Reading 2	Pressure, Reading 1	Difference (g)	Absolute stress $(\sigma_i + g)$
1 ...	300	300	0	412
2 ...	600	500	+100	512
3 ...	800	700	+100	512
4 ...	500	300	+200	612
5 ...	700	400	+300	712
6 ...	700	200	+500	912

7. Plot absolute stresses as shown in figure 14*B*.

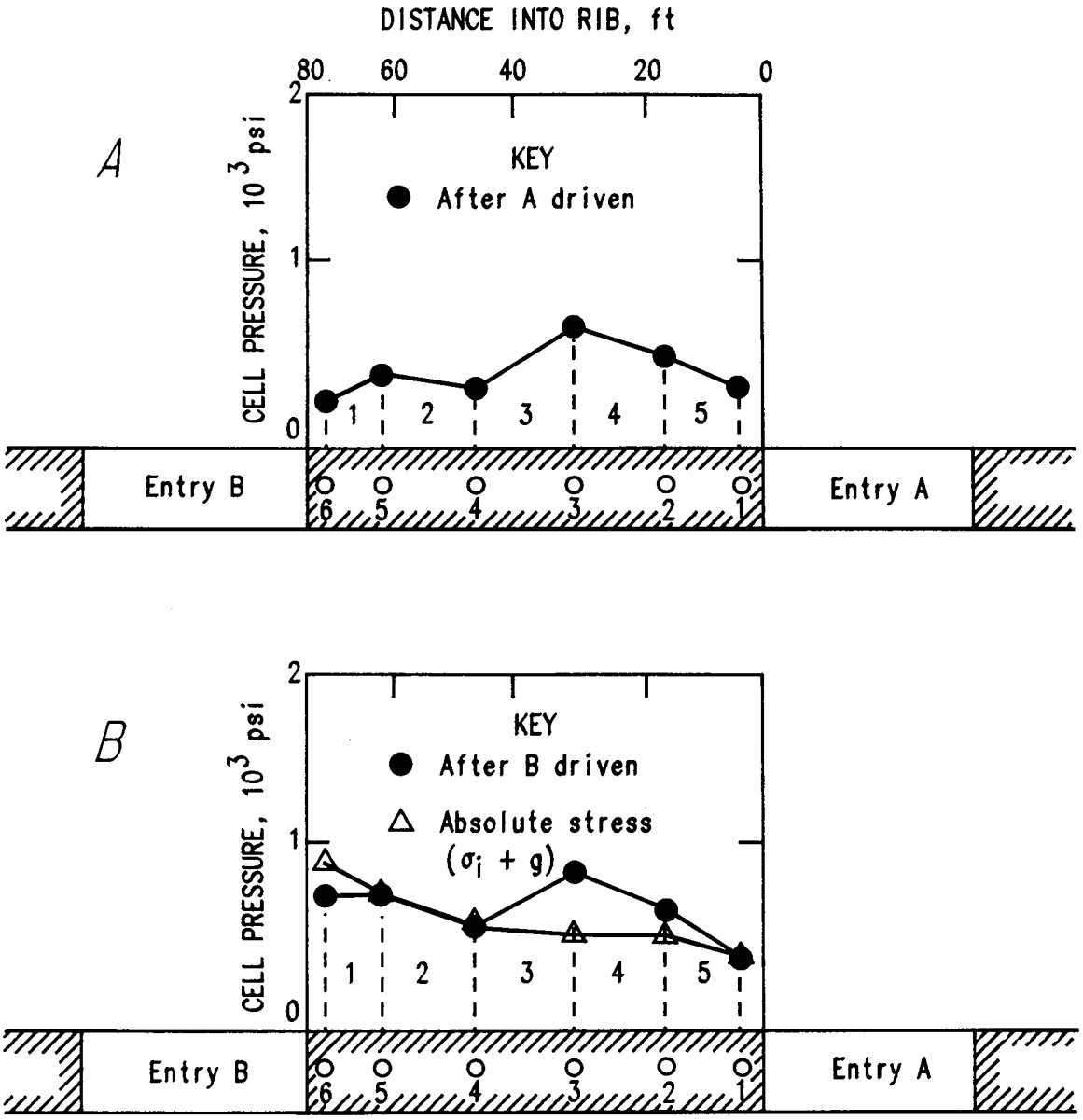

Figure 14.—Example illustrating static equilibrium method. *A*, Example pressure cell readings prior to driving entry; *B*, postentry development pressure cell readings and absolute stress values. Zones are numbered left to right; cells are numbered right to left.

Figure 15 illustrates use of the static equilibrium approach to determine the absolute stress distribution resulting from widening an existing opening: Curve 1 shows the initial pressure cell readings; curve 2 represents the postwidening readings. Equating the areas under the two curves,

$$\text{where } (A_1 - A_3) = \sigma_i w_1/2,$$

$$\text{and } (A_2 - A_3) = \sigma_i w_2/2,$$

$$\text{yields } (A_2 - A_1) = \sigma_i(w_2 - w_1)/2. \quad (4)$$

The factor 1/2 is used because the areas for only one side of the opening are considered. Pressure cell measurements provide the stress changes (g) for determining the area $(A_2 - A_1)$. Given this area and the opening widths, w_1 and w_2, equation 4 is solved for the initial stress, σ_i.

Sellers (*27*), using elastic theory, derived equations for converting observed cell pressure changes to rock stress changes. This method requires the elastic properties of the rock and the borehole instrument stiffness, with instrument stiffness being derived from cell pressurization cycles in a borehole. Rock properties can be obtained from either laboratory or in situ modulus of rigidity tests. The in situ test assumes a value for Poisson's ratio.

The CPC can sense ground pressure changes that exert a uniform radial pressure against the borehole wall, but cannot distinguish between vertical and horizontal rock stress changes (*4, 28*). Using CPC data, rock stress changes (fig. 16*A*) are determined by the following equations:

$$(\Delta S + \Delta T) = \frac{\Delta P_{cpc} C_S E}{2\pi L a^2} \text{ (plane stress condition)} \quad (5)$$

or

$$(\Delta S + \Delta T) = \frac{\Delta P_{cpc} C_S E}{2\pi L a^2 (1-\upsilon^2)} \text{ (plane strain condition)}, \quad (6)$$

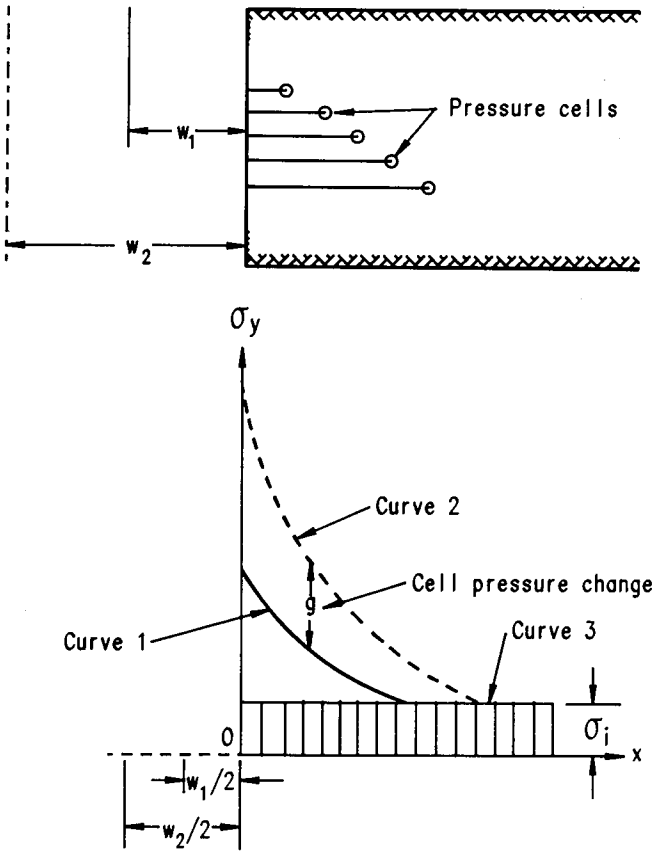

Figure 15.—Vertical stress determination after widening existing opening.

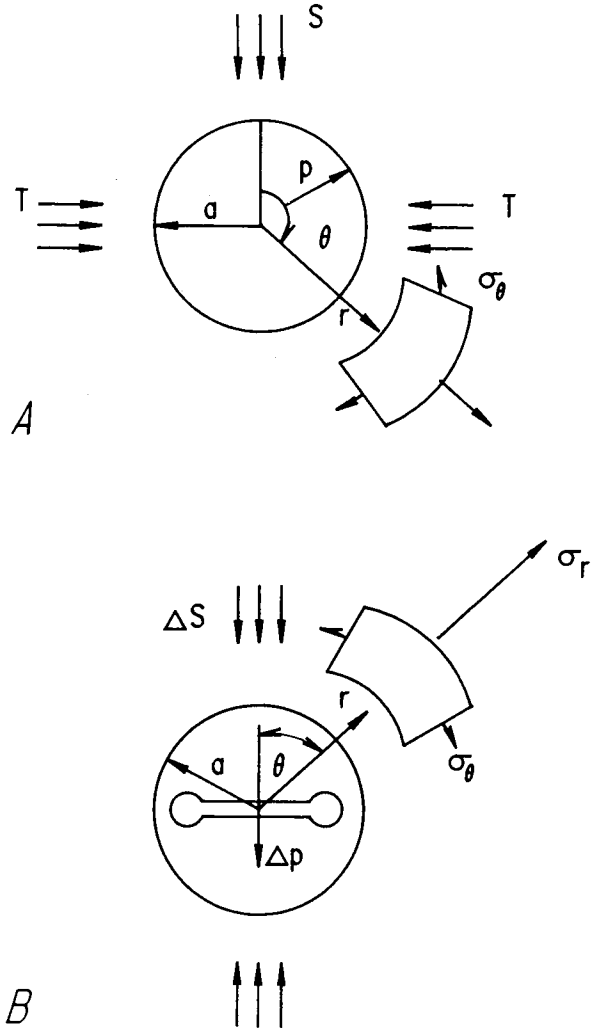

Figure 16.—Stress around CPC exerting uniform radial pressure (*A*) and stress around BPC on borehole wall (*B*).

where ($\Delta S = \Delta T$) = vertical and horizontal stress changes, respectively,

ΔP_{cpc} = observed CPC pressure change,

E = elastic modulus of rock,

L = CPC length,

a = borehole radius,

υ = Poisson's ratio of rock,

and C_S = cell and system stiffness from expansion test.

Vertical rock stress changes can be determined from the BPC's, flatjack cells responding to ground pressure changes normal to the plane of the cell (fig. 16*B*). Using similar expressions, rock stress changes for the plane stress and plane strain conditions are determined by applying the following equations:

$$\Delta S = \frac{\Delta P_{cpc} C_S E}{2\pi L a^2 (1-\upsilon^2)} \text{ (plane strain condition)} \quad (7)$$

or

$$\Delta S = \frac{\Delta P_{cpc} C_S E}{2\pi L a^2} \text{ (plane stress condition)}, \quad (8)$$

where ΔS = stress change perpendicular to flatjack plane.

Lu (*10, 29-31*) has developed a direct rock stress measurement technique, especially suited for weak and soft rock. In situ rock stresses are calculated from either a three-cell package (one CPC and two orthogonally oriented BPC's) or, if the local rock response ratio is known, a two-BPC package (*31*). The biaxial rock stresses are determined by solving equations for the sum of the stresses from the CPC readings and for the ratio of the stresses from the BPC readings. Lu (*29*) includes detailed theoretical considerations, equation derivations, and the basic concepts of mining-induced stress measurement. Example 2 shows cell data and the necessary calculations.

EXAMPLE 2: This example illustrates the use of Lu's method to determine response ratio and mining-induced stresses using mine data from a three-cell package (*10, 29*).

Day	Pressure cell readings			Premining and postmining ground stresses	
	P_{bpv}	P_{bph}	P_{cpc}	N_v	N_h
34 . . .	1,800	1,700	1,800		
42 . . .	1,800	1,700	1,900	1,233	1,135
56 . . .	1,800	1,700	1,900	1,302	1,198
63 . . .	1,800	1,500	2,000	1,490	1,142
70 . . .	1,900	1,400	2,000	1,606	1,026
77 . . .	1,900	1,400	2,000	1,606	1,026
85 . . .	1,900	1,400	2,000	1,606	1,026
94 . . .	1,900	1,400	1,900	1,525	975
100 . .	1,900	1,500	2,100	1,619	1,144
107 . .	1,900	1,400	2,100	1,686	1,077
114 . .	2,000	1,400	2,200	1,820	1,075
121 . .	1,500	1,300	1,900	1,380	1,120
128 . .	1,400	1,200	1,900	1,389	1,111

1. Premining ground stress determination:

At day 34:

$P_{e\text{-}bpv} = 1{,}800$

$P_{e\text{-}bph} = 1{,}700$

$P_{e\text{-}cpc} = 1{,}800$

$S_c = 0.185$

$$Q = \frac{P_{e\text{-}bph}}{P_{e\text{-}bpv}} = \frac{1{,}700}{1{,}800} = 0.944.$$

$$N_1 + N_2 = \frac{P_{e\text{-}cpc}}{(1-\nu)} = \frac{1{,}800}{0.76} = 2{,}368.$$

$$\frac{N_1}{N_2} = \frac{Q - S_c}{1 - QS_c} = \frac{0.944 - 0.185}{1 - 0.944(0.185)} = \frac{0.759}{0.825} = 0.920.$$

$$N_1 = 0.92N_2$$

$$N_1 + N_2 = 2{,}368$$

$$1.92N_2 = 2{,}368$$

N_2 (vertical stress) = 1,233 psi

N_1 (horizontal stress) = 1,135 psi

2. Response ratio, K, determination:

At equilibrium:

$$P_{e\text{-}bpv} = 1{,}800$$
$$P_{e\text{-}bph} = 1{,}700$$
$$N_v = 1{,}233$$
$$N_h = 1{,}135$$

$$K = \frac{P_{e\text{-}bpv}}{N_v + S_c N_h} = \frac{1{,}800}{1{,}233 + 0.185(1{,}135)} = \frac{1{,}800}{1{,}442} = 1.247.$$

or

$$K = \frac{P_{e\text{-}bph}}{N_h + S_c N_v} = \frac{1{,}700}{1{,}135 + 0.185(1{,}233)} = \frac{1{,}700}{1{,}363} = 1.247.$$

3. Postmining ground stress determination:

At day 100:

$$P_{bpv} = 1{,}900$$
$$P_{bph} = 1{,}500$$

$$N_v = \frac{P_{pbv} - S_c(P_{bph})}{K(1 - S_c^2)} = \frac{1{,}900 - 0.185(1{,}500)}{1.247\{1 - (0.185)^2\}}$$

$$= \frac{1{,}622}{1.204} = 1{,}348.$$

$$N_h = \frac{P_{pbh} - S_c(P_{bpv})}{K(1 - S_c^2)} = \frac{1{,}500 - 0.185(1{,}900)}{1.247\{1 - (0.185)^2\}}$$

$$= \frac{1{,}149}{1.204} = 954.$$

As shown in example 2, premining ground stresses can be determined by solving the following equations (*10, 29*):

$$N_1 + N_2 = \frac{P_{e\text{-}cpc}}{(1 - \upsilon)}, \tag{9}$$

and

$$\frac{N_1}{N_2} = \frac{Q - S_c}{1 - QS_c}, \tag{10}$$

where $P_{e\text{-}cpc}$ = CPC equilibrium pressure,

υ = Poisson's ratio (assumed 0.24),

Q = ratio of horizontal and vertical BPC equilibrium pressures (0.944),

S_c = BPC transverse sensitivity (0.185),

and N_1, N_2 = preexisting biaxial ground stresses.

Figure 17 shows cell pressure data and calculated rock stress versus time. The pressure could also be plotted versus face distance from the cells.

Following calculations of the premining ground stresses, the response ratio, K, can be calculated using the following equations (*30-31*):

$$K = \frac{P_{e\text{-}cpc} - P_{e\text{-}bpv}}{N_1 + S_c N_2} \tag{11}$$

or

$$K = \frac{P_{e\text{-}cpc} - P_{e\text{-}bph}}{N_2 + S_c N_1}, \tag{12}$$

where $P_{e\text{-}bpv}$, $P_{e\text{-}bph}$ = BPC vertical and horizontal equilibrium pressures.

Mining-induced stresses can then be determined from two BPC readings, using their known K values, or with the two-cell package consisting of two BPC's oriented perpendicular to each other. Example 3 and figure 18 illustrate use of this technique using BPC data from an underground coal mine.

EXAMPLE 3: This example illustrates the use of Lu's method to determine mining-induced stresses using mine data from a two-cell package. Pressure cell readings and stresses determined, in pounds per square inch:

Day	*Pressure cell readings*		*Mining-induced stresses*	
	P_{bpv}	P_{bph}	N_v	N_h
140 . .	2,500	900	1,938	363
146 . .	2,600	900	2,021	348
152 . .	2,600	1,000	2,081	431
160 . .	2,700	1,200	2,058	582
180 . .	2,900	1,400	2,194	717

K, from a three-cell site, = 1.247.

If the measured biaxial stresses are vertical and horizontal, then mining-induced vertical and horizontal stresses can be calculated from the following equations, which were derived from equations 11 and 12:

$$N_v = \frac{P_{bpv} - S_c(P_{bph})}{K(1 - S_c^2)} \tag{13}$$

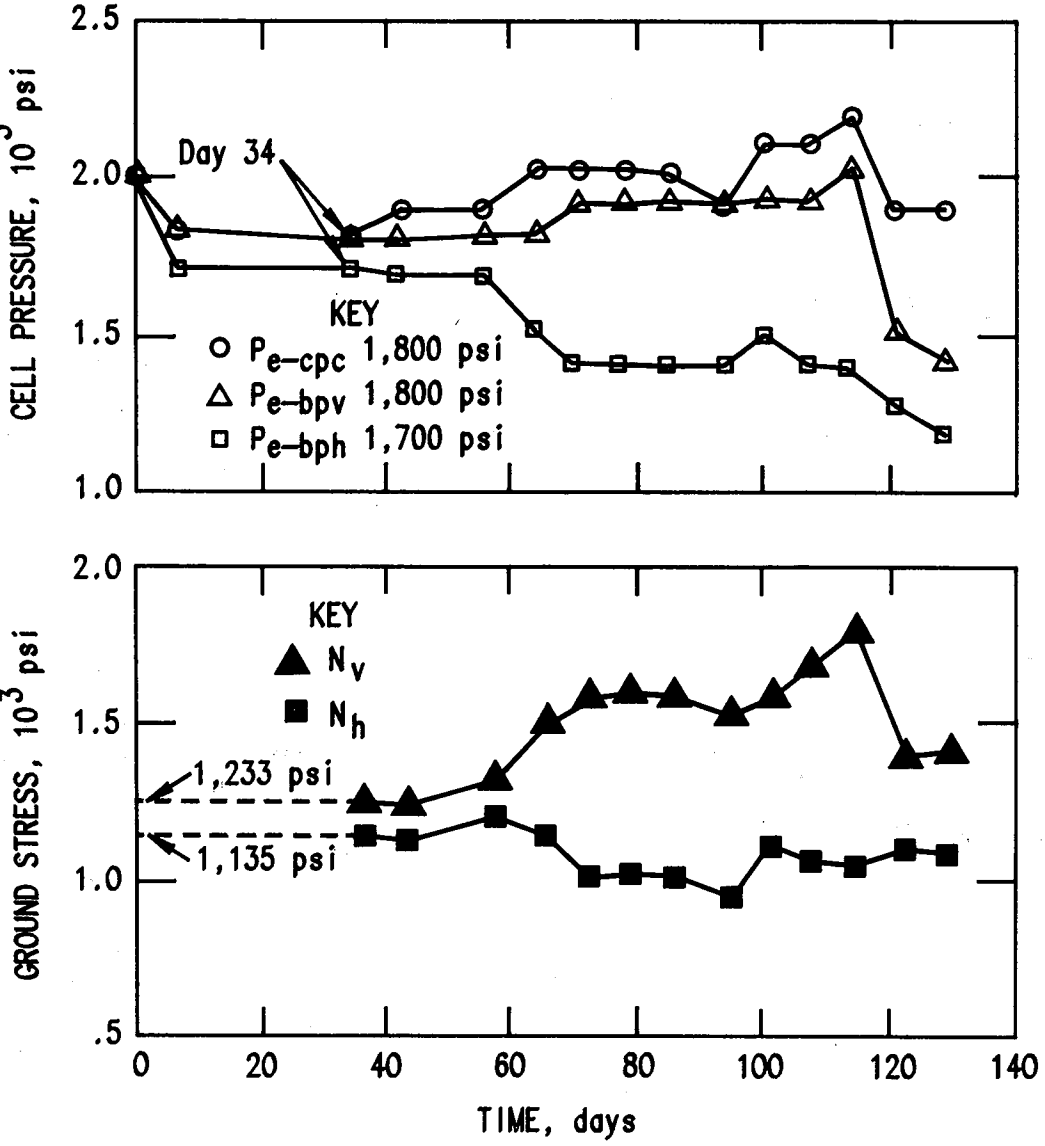

Figure 17.—Cell and ground pressures versus time from three-cell package.

and $$N_h = \frac{P_{bph} - S_c(P_{bpv})}{K(1 - S_c^2)}, \quad (14)$$

where N_h, N_v = mining-induced horizontal and vertical stresses,

and P_{bph}, P_{bpv} = horizontal and vertical BPC readings.

Babcock (*32*), from experimental testing, derived equations for converting BPC pressure changes to biaxial ground stress changes. Laboratory results showed that the logarithm of cell pressure change is proportional to rock stress change; cell response increases with increased setting pressure; cell response decreases with increased rock stiffness; and cell sensitivity to transverse loading exceeds earlier reported values.

For calculating biaxial stress state, Babcock derived the following equations:

$$S_v = \frac{3}{8m} \ln \left[\left(\frac{\sigma_v}{\sigma_v^*} \right)^3 \left(\frac{\sigma_h}{\sigma_h^*} \right) \right], \quad (15)$$

$$S_h = \frac{3}{8m} \ln \left[\left(\frac{\sigma_h}{\sigma_h^*} \right)^3 \left(\frac{\sigma_v}{\sigma_v^*} \right) \right], \quad (16)$$

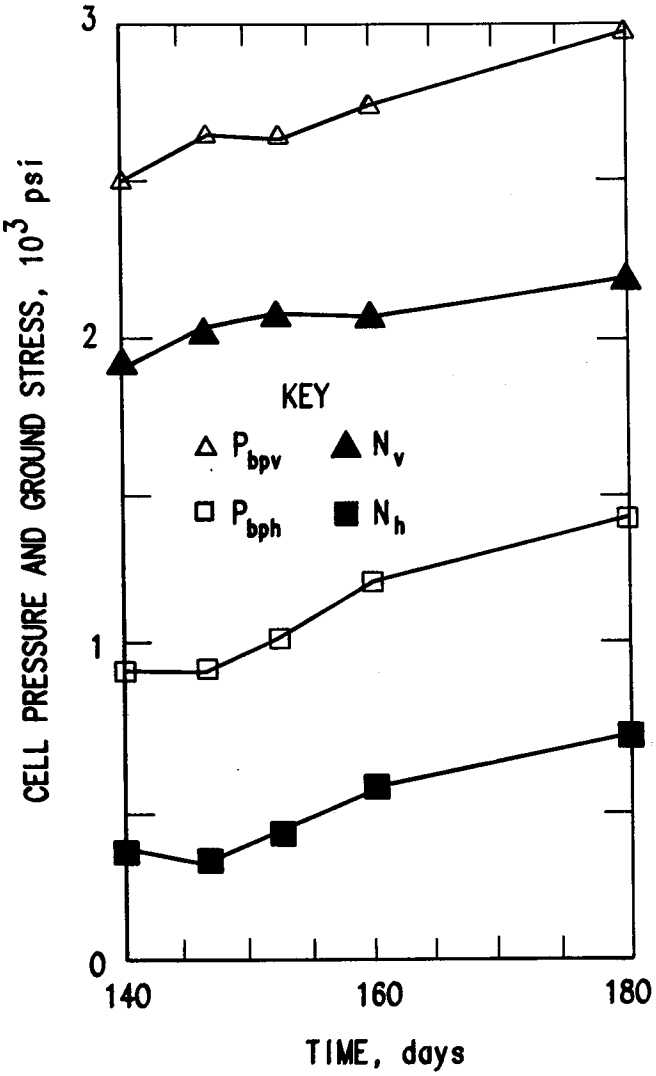

Figure 18.—Cell pressure and ground stress versus time from two-cell package.

$$m\ (psi) = 4.348 \left[\frac{1-\nu^2}{E}\right]^{2/3}, \quad (17)$$

and

$$m\ (GPa) = 0.220 \left[\frac{1-\nu^2}{E}\right]^{2/3}, \quad (18)$$

where S_v, S_h = vertical and horizontal rock stress change,

σ_v^*, σ_h^* = vertical and horizontal BPC setting pressures,

σ_v, σ_h = vertical and horizontal BPC pressure readings,

m = slope of laboratory-derived equations relating pressure cell and rock pressure change to cell setting pressure,

E = elastic modulus of rock,

and υ = Poisson's ratio of rock.

Absolute stresses can be determined by adding the computed rock stress changes to the preexisting stress field. Example 4 and figure 19 illustrate this technique, using data from pressure cells installed in a longwall panel.

EXAMPLE 4: This example illustrates Babcock's method to determine mining stress changes using mine data from vertical and horizontal cell pressure. Units are pounds per square inch:

Face distance, ft	Vertical			Horizontal		
	P_{bpv}	ΔP_{pbv}	S_v	P_{bph}	ΔP_{bph}	S_h
175	1,500	0	0	1,500	0	0
150	1,595	95	77	1,515	15	36
75	1,655	155	122	1,520	20	55
50	1,740	240	186	1,540	40	90
25	2,155	655	432	1,510	10	151
15	2,500	1,000	611	1,522	22	219

IN SITU PHYSICAL PROPERTIES FROM CELL DATA

Hydraulic borehole pressure cells can also be used to determine in situ physical properties. The CPC was originally developed to determine in situ values for the modulus of rigidity. Panek (*28*) provides an explanation of theoretical considerations, data reduction, and comparison of CPC test results with other methods.

Test procedures require CPC calibration within two metal cylinders, determination of pressure-volume characteristics for the PCM, and CPC expansion inside a borehole to determine the in situ modulus of rigidity. Borehole diameter change is proportional to the fluid volume pumped into the CPC. To accurately determine fluid volume, two or sometimes three calibration tests are performed. These calibration tests provide two constants and account for factors such as fluid compressibility, CPC end effects and copper shell expansion, and expansion of the tubing and other hardware. Testing requires cyclic pressurization of the CPC, typically two cycles. The CPC is pressurized first within one of the calibration cylinders; the procedure is repeated for the second cylinder; and finally, the pressure-volume cycling is performed in the borehole. Figure 20 shows a typical CPC calibration curve; the slope of the pressure-volume curve is essential. One turn on the PCM equals 0.0192 in^3 (*28*).

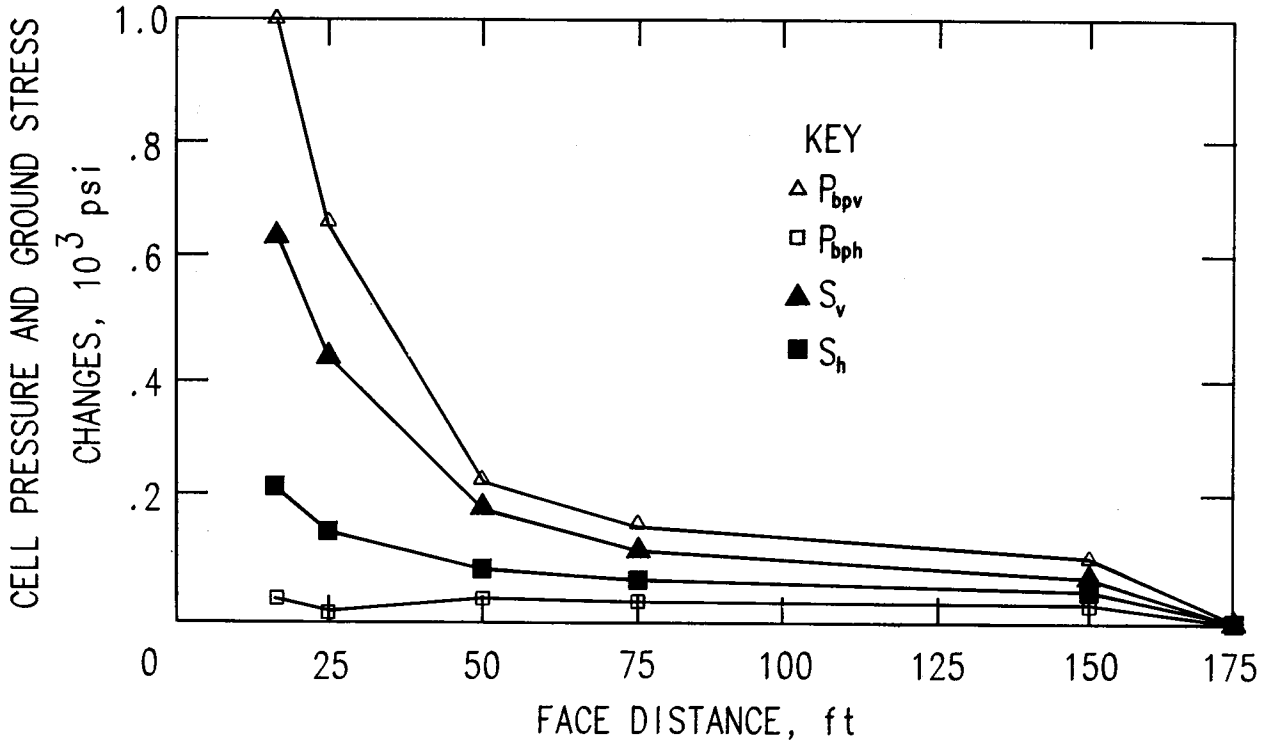

Figure 19.—Cell pressure and ground stress changes versus face distance.

Expansion of the CPC against either a calibration cylinder or drill-hole wall provides a value for $\Delta V/\Delta p$, where ΔV is the volume change resulting from PCM piston displacement and Δp is the change in fluid pressure. The relationship between $\Delta V/\Delta p$ and $\Delta V_i/P_i$ at the borehole or inner cylinder wall is (*28*)

$$\left[\frac{\Delta V_i}{P_i}\right]_{\substack{\text{cylinder or}\\ \text{borehole}}} = \alpha + \beta \left[\frac{\Delta V}{\Delta p}\right]_{PCM}. \quad (19)$$

Constant α corrects for fluid volume changes not due to hole diameter changes, while β corrects for the fact that fluid pressure is not transmitted undiminished to the calibration cylinder or borehole wall. A small portion expands the copper shell of the CPC (*28*).

$$\left[\frac{2\pi r_i L}{E/R}\right]_{\substack{\text{cylinder or}\\ \text{borehole}}} = \alpha + \beta \left[\frac{\Delta V/\Delta T_p}{\Delta p/\Delta T_p}\right]_{PCM}. \quad (20)$$

The term $\Delta V/\Delta T$, 0.0192 in^3 per PCM piston turn, is a constant. The slope of the pressure-volume curve depends on the constants α and β and on the ratio E/R specific

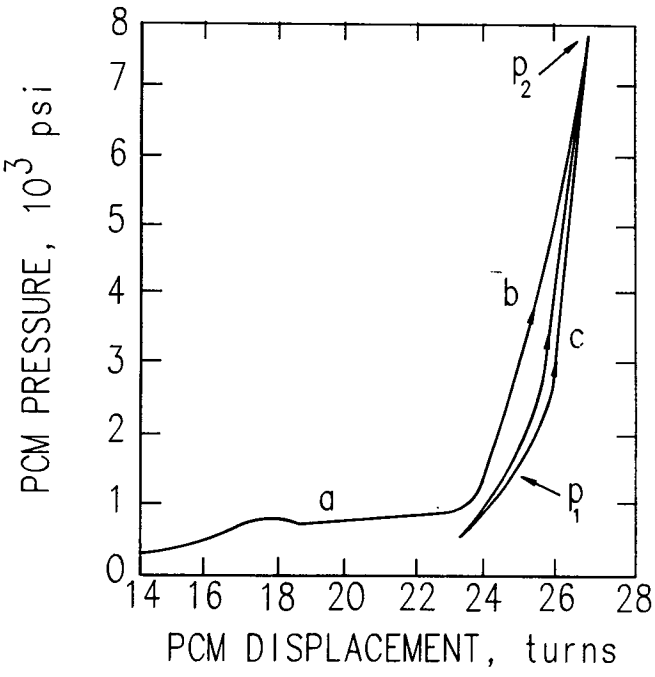

Figure 20.—PCM pressure versus PCM displacement. Path a represents expansion of CPC copper shell, while path b represents cylinder or borehole dilation. Pressure decrease is shown on path c. Path c slope is steeper than path b slope because only elastic strain is recovered. Subsequent pressure cycles tend to follow path c.

to each calibration cylinder. Determination of the constants, α and β, and the modulus of rigidity, G, requires solving the following equations:

$$\epsilon = \frac{2\pi r_i}{E/R}, \quad (21)$$

$$\xi = \Delta V/\Delta T_p, \quad (22)$$

$$\eta = \Delta p/\Delta T_p. \quad (23)$$

Substituting equations 21-23 into equation 20 yields (*28*)

$$\beta = \frac{(\epsilon_1 - \epsilon_2)L}{\xi} \times \frac{\eta_1\eta_2}{\eta_2 - \eta_1}, \quad (24)$$

and

$$\alpha = \epsilon_1 L - \beta\xi/\eta_1, \quad (25)$$

where α, β = calibration constants,

ϵ_1, ϵ_2 = constants for the two calibration cylinders used,

ξ = 0.0192 in^3 per PCM piston turn,

L = CPC effective length (7 in),

r_i = inside radius of cylinder,

and η_1, η_2 = pressure-volume slopes from calibration tests.

Expansion of the CPC in a borehole provides a new pressure-volume slope, m_3, which with the above calculated constants, α and β, determines the modulus of rigidity, G,

$$G = \frac{\pi r_3^2 L}{a + \beta\xi/\eta_3}, \quad (26)$$

where G = in situ modulus of rigidity,

η_3 = pressure-volume slope from test in borehole,

and

$$r_3^2 = r_i^2 + \frac{\xi(T_3 - T_1)}{\pi L}, \quad (27)$$

where r_i = inner radius of calibration cylinder number 1,

and $T_3 - T_1$ = difference in PCM turns at 1,000 psi between test in borehole and test in calibration cylinder number 1.

The following detailed example and figure 21 will clarify the use of this method.

EXAMPLE 5: This example illustrates the determination of modulus of rigidity from CPC calibration curves. Specifications for calibration cylinders used in this example are as follows:

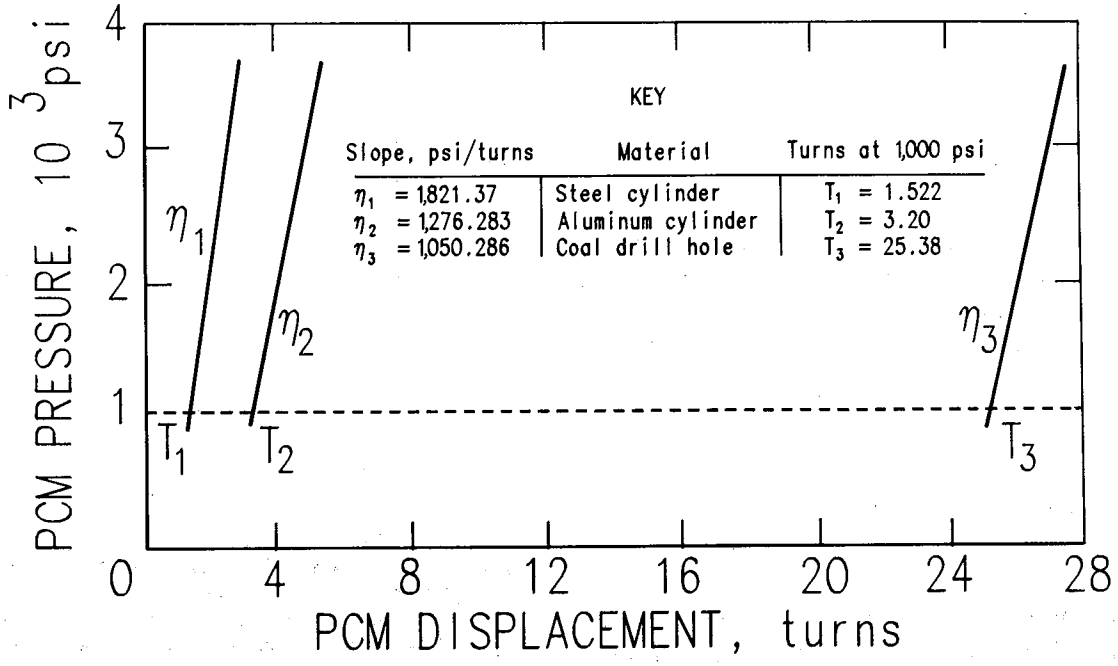

Figure 21.—Example calibration curves for determining in situ modulus of rigidity.

	Cylinder 1	Cylinder 2
E ..... 10^6 psi ..	30.37	10.50
υ	0.294	0.343
Inner radius ..... in ..	0.740	0.741
Outer radius ..... in ..	1.047	0.998
γ/ρ ..... lb/in^3 ..	12,741	3,960
ϵ ..... 10^{-6} in^4/lb ..	0.3649	1.1757
Material	Steel	Aluminum

CPC pump-up tests were performed in an underground coal mine to determine the in situ modulus of rigidity, G. Figure 21 shows second-cycle slopes for expansion tests in the two calibration cylinders and in a drill hole in the coal seam. Using data from the above pressure-turns plot and calibration cylinder specifications, G is determined as follows:

1. Determine constant β (equation 24):

$$\beta = \frac{(\epsilon_1 - \epsilon_2)L}{\xi} \times \frac{\eta_1\eta_2}{\eta_2 - \eta_1}$$

$$= \frac{(0.3649 - 1.1757 \times 10^{-6})(7.125)}{0.0190}$$

$$\times \frac{(1{,}821.37)(1{,}276.283)}{(1{,}276.283) - (1{,}821.37)} = 1.2967.$$

2. Determine constant α (equation 25):

$$\alpha = \epsilon_1 L - \beta\xi/\eta_1 = (0.3649 \times 10^6)(7.125)$$

$$- \frac{(1.2967)(0.019)}{1{,}821.37} = -1.093 \times 10^{-5}.$$

3. Determine r_3^2 (equation 27):

$$r_3^2 = r_1^2 + \frac{\xi(T_3 - T_1)}{\pi L} = \frac{0.019(25.38 - 1.52)}{\pi(7.125)}$$

$$+ (0.740)^2 = 0.568\ \text{in}^2.$$

$$r_3^2 = r_2^2 + \frac{\xi(T_3 - T_2)}{\pi L} = \frac{0.019(25.38 - 3.2)}{\pi(7.125)}$$

$$+ (0.741)^2 = 0.568\ \text{in}^2.$$

$$r_3^2(\text{av}) = 0.568\ \text{in}^2.$$

4. Calculate G (equation 26):

$$G = \frac{\pi r_3^2 L}{\alpha + \beta\xi/\eta_3} = \frac{\pi(0.568)(7.125)}{1.093 \times 10^{-5} + (1.2967)/1{,}050.286}$$

$$= 1.015 \times 10^6.$$

Lu (*33-34*) recently proposed a new method for the in situ determination of the modulus of deformation and Poisson's ratio. These properties are determined from the previously described combination of one CPC and two BPC's installed in a single borehole (three-cell package) (*35*). Lu (*31, 33-34*) also includes discussion of theoretical considerations, brief descriptions of other available in situ physical properties tests, and examples of this technique. The deformation modulus is determined by (*33-34*)

$$E_r = \frac{2\pi a^2 L(1 + \nu_r)}{P_{cpc}}\left[(1 - \nu_r)(N_1 + N_2) - P_{e\text{-}cpc}\right]/C, \quad (28)$$

where E_r = rock mass deformation modulus (secant),

υ_r = rock mass Poisson's ratio (secant),

P_{cpc} = CPC pressure reading,

$P_{e\text{-}cpc}$ = CPC equilibrium pressure,

a = CPC drill-hole radius,

N_1, N_2 = biaxial stresses as determined using equations 9-10,

and

$$C = k_1 + k_2(V_c/P_c), \quad (29)$$

where k_1 = constant related to fluid volume retained in CPC,

k_2 = constant related to response ratio between input and output of CPC pressure,

V_c = fluid volume change in CPC for each turn of PCM piston,

and P_c = fluid pressure change in CPC for each turn of PCM piston.

Poisson's ratio is determined by using (*33-34*)

$$\frac{\nu_r}{(1-\nu_r)} = \frac{(N_2 - N_{2\text{-}0})}{(N_1 - N_{1\text{-}0})}, \qquad (30)$$

where υ_r = in situ Poisson's ratio (secant),

$N_{1\text{-}0}$, $N_{2\text{-}0}$ = biaxial stresses at equilibrium,

and N_1, N_2 = biaxial stresses (N_1 is imposed and N_2 is induced by Poisson's effect).

The constants, k_1 and k_2, correspond to α and β (*28*) and are calculated as shown in equations 24 and 25. If P_{cpc}, $P_{e\text{-}cpc}$, N_1, N_2, and υ_r are known, E_r is calculated using equation 28. Poisson's ratio is determined from the biaxial stresses calculated from equations 13 and 14, and from the biaxial stresses at equilibrium, $N_{1\text{-}0}$ and $N_{2\text{-}0}$. These equilibrium biaxial stresses can be calculated from equations 9 and 10 using an iterative method; a Poisson's ratio value is first assumed, and the stress values corrected using the in situ value for υ_r (*33-34*).

Results of this technique are illustrated in figure 22 (*33*). Example 3 and figure 18 show indicated pressure readings and calculated biaxial stresses. Poisson's ratio was calculated using equation 30, and for each set of υ_r, ΔP_{cpc}, N_1, and N_2, E_r was calculated from equation 28. Figure 22 is shown as a function of the normalized axial stress, Z/Z_0, with $Z = N_1$ and $Z_0 = N_{1\text{-}0}$ (*33*).

Babcock (*32*) also includes a technique for the in situ determination of Poisson's ratio. Pressure cells are installed to the same setting pressure to measure both horizontal and vertical pressure changes. The ratio of horizontal to vertical pressure changes are used with figure 23 to estimate Poisson's ratio (*32*).

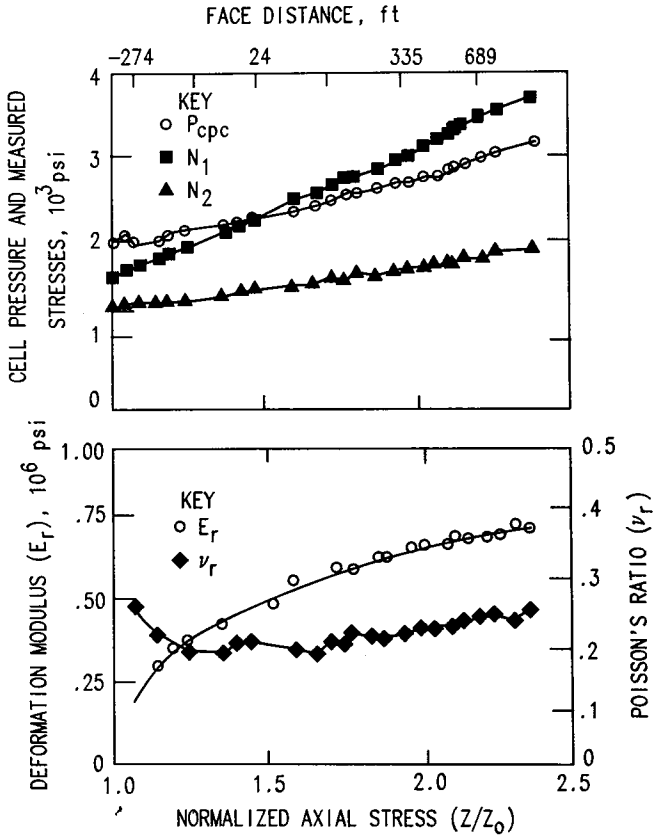

Figure 22.—In situ deformation modulus and measured stresses versus normalized axial stresses (33).

SUMMARY AND CONCLUSIONS

Hydraulic borehole pressure cells have been utilized for several decades to investigate strata control problems and to perform in situ physical properties tests. Various designs and techniques have been developed by different investigators. This report summarizes usage of pressure cells and techniques developed by Bureau personnel. It includes information required for the construction and installation of pressure cells and analyses of pressure cell data. Analyses included a summary of results from field studies, as well as procedures required for converting cell pressures to ground stresses and changes in ground stress, and step-by-step procedures for in situ physical property testing.

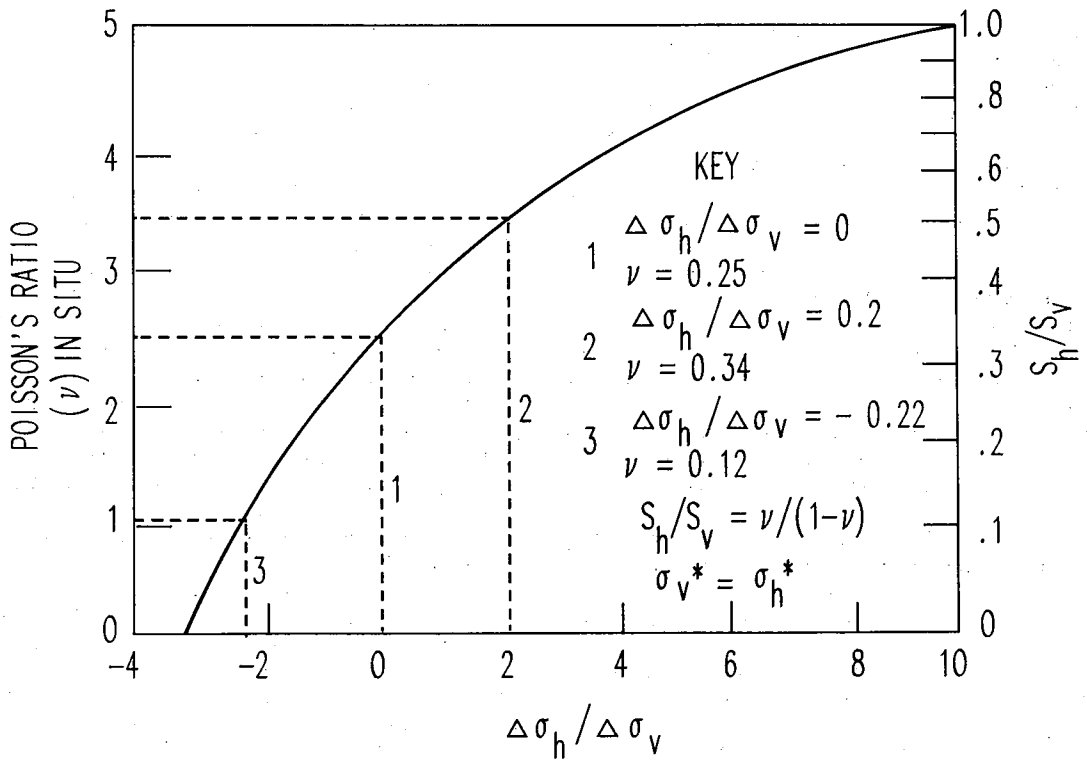

Figure 23.—In situ Poisson's ratio based on the absolute stress change technique (32).

REFERENCES

1. Panek, L. A. Measurement of Rock Pressure With a Hydraulic Cell. Min. Eng. (N.Y.), v. 13, 1961, pp. 282-285.

2. Panek, L. A., and J. A. Stock. Pressure Control Mechanism. U.S. Pat. 3,108,716, Oct. 29, 1963.

3. U.S. Bureau of Mines. Combination Bit Rapidly Drills Precision Boreholes in Soft Rock. Technol. News, No. 152, 1982, 2 pp.

4. Panek, L. A. Solution of Mine Structure Problems Through Field Measurements and Theoretical Analysis. Paper in Rock Mechanics Instrumentation for Mine Design. BuMines IC 8585, 1973, pp. 23-34.

5. Panek, L. A., and J. A. Stock. Development of a Rock Stress Monitoring Station Based on the Flat Slot Method of Measuring Existing Rock Stress. BuMines RI 6537, 1964, 61 pp.

6. Miller, T. C., and R. Sporcic. Development of a Hydraulic Device for Measuring Relative Pressure Changes in Coal During Mining: A Progress Report. BuMines RI 6571, 1964, 13 pp.

7. Mudra, P. J., and R. Sporcic. Encapsulated Hydraulic Cells for Measuring Pressure Changes in Coal. Trans. Soc. Min. Eng. AIME, v. 226, 1963, pp. 396-401.

8. Barry, A. J., A. Zona, J. L. Gilley, and R. H. Oitto, Jr. Investigation of Stress Distributions in Burst-Prone Coal Pillars. BuMines RI 6971, 1967, 12 pp.

9. Curth, E. A. Relative Pressure Changes in Coal Pillars During Extraction: A Progress Report. BuMines RI 6980, 1967, 20 pp.

10. Lu, P. H. Ground Control Study of a Mechanized Longwall Coal Operation in West Virginia. BuMines RI 8929, 1985, 34 pp.

11. Harza Engineering Co. Comprehensive Ground Control Study of a Mechanized Longwall Operation. Final Report (contract H0230012). BuMines OFR 5(1)-77, 1976, 151 pp.; OFR 5(2)-77, 1976, 270 pp.; NTIS PB 262-475, 476.

12. Moebs, N. N., and E. A. Curth. Geologic and Ground Control Aspects of an Experimental Shortwall Operation in the Upper Ohio Valley. BuMines RI 8112, 1976, 30 pp.

13. Lu, P. H. Rock Mechanics Instrumentation and Monitoring for Ground Control Around Longwall Panels. Paper in International Symposium on State-of-the-Art of Ground Control in Longwall Mining and Subsidence (Honolulu, HI, Sept. 1982). Soc. Min. Eng. AIME, 1982, pp. 159-166.

14. Allwes, R. A., J. M. Listak, G. J. Chekan, and D. R. Babich. The Effects of a Retreating Longwall on a Three-Entry Gate Road System. BuMines RI 8996, 1985, 19 pp.

15. DeMarco, M. J., J. R. Koehler, and P. H. Lu. Characterization of Chain Pillar Stability in a Deep Western Coal Mine—Case Study. Min. Eng. (Littleton, CO), v. 40, 1988, pp. 1115-1119.

16. Kripakov, N. P., L. A. Beckett, and D. A. Donato. Loading on Underground Mine Structures Influenced by Multiple Seam Interaction. Paper in International Symposium on Application of Rock Characterization Techniques in Mine Design (SME-AIME Annu. Meet., New Orleans, LA, Mar. 1986). Soc. Min. Eng. AIME, 1986, pp. 225-236.

17. Kneisley, R. O. Rock Mechanics Investigation of Two-Bed Trona Mining, Green River, Wy. BuMines RI 8598, 1982, 22 pp.

18. Matetic, R. J., G. J. Chekan, and J. A. Galek. Pillar Load Transfer Associated With Multiple-Seam Mining. BuMines RI 9066, 1987, 23 pp.

19. Hackett, T. D., and H. Park. Ground Control Analysis of Multi-Slice Mining for Thick Western Coal Seams. Soc. Min. Eng. AIME preprint 87-39, 1987, 7 pp.

20. Campoli, A. A., C. A. Kertis, and C. A. Goode. Coal Mine Bumps: Five Case Studies in the Eastern United States. BuMines IC 9149, 1987, 34 pp.

21. Haramy, K. Y., R. O. Kneisley, and J. P. McDonnell. Longwall Face Bursts and Inadequate Caving: A Case Study. Paper in Proceedings of 6th International Conference on Ground Control in Mining. WV Univ., Morgantown, WV, 1987, pp. 18-31.

22. Haramy, K. Y., R. O. Kneisley, and B. T. Brady. Analysis of a Major Failure Through Integration of Static and Dynamic Rock Mechanics Instrumentation. Paper in Proceedings of 7th International Conference on Ground Control in Mining. WV Univ., Morgantown, WV, 1988, pp. 218-227.

23. Kripakov, N. P. Analysis of Pillar Stability on Steeply Pitching Seam Using the Finite Element Method. BuMines RI 8579, 1981, 33 pp.

24. Kripakov, N. P., and M. J. DeMarco. Case Study: Gateroad Performance in Deep Western Coal Mine. Paper in Proceedings of 3rd Annual International Conference and Exhibition on Longwall Mining (Pittsburgh, PA, 1988). Industrial Presentations, Inc., Aurora, CO, 1988, pp. 167-185.

25. Heasley, K. A., and K. Barron. A Case Study of Gate Road Response to Longwall Mining in Bump-Prone Strata. Paper in Proceedings of 3rd Annual International Conference and Exhibition on Longwall Mining (Pittsburgh, PA, 1988). Industrial Presentations, Inc., Aurora, CO, 1988, pp. 91-106.

26. Morgan, T. A., and L. A. Panek. A Method for Determining Stress in Rock. BuMines RI 6312, 1963, 7 pp.

27. Sellers, J. B. The Measurement of Rock Stress Changes Using Hydraulic Borehole Gages. Int. J. Rock Mech. and Min. Sci., v. 7, 1970, pp. 423-435.

28. Panek, L. A., E. E. Hornsey, and R. L. Lappi. Determination of the Modulus of Rigidity of Rock by Expanding a Cylindrical Pressure Cell in a Drillhole. Paper in Proceedings of Sixth Symposium on Rock Mechanics. Univ. MO, Rolla, MO, 1964, pp. 427-449.

29. Lu, P. H. Determination of Ground Pressure Existing in a Viscoelastic Rock Mass by Use of Hydraulic Borehole Pressure Cells. Paper in Proceedings of International Symposium on Weak Rock (Tokyo, Japan, 1981). Balkema, 1981, v. 1, pp. 459-465.

30. ____. Mining-Induced Stress Measurement With Hydraulic Borehole Pressure Cells. Paper in Proceedings of 25th U.S. Symposium on Rock Mechanics. Northwest. Univ., Evanston, IL, 1984, pp. 204-211.

31. ____. A New Method of Rock Stress Measurement With Hydraulic Borehole Pressure Cells. Paper in Proceedings of International Symposium on Rock Stress and Rock Stress Measurements. (Stockholm, 1986). CENTEK, 1986, pp. 237-245.

32. Babcock, C. O. Equations for the Analysis of Borehole Pressure Cell Data. Paper in Proceedings of the 27th U.S. Symposium on Rock Mechanics. Univ. AL, Tuscaloosa, AL, 1986, pp. 512-519.

33. Lu, P. H. In Situ Determination of Deformation Modulus and Poisson's Ratio of a Rock Mass With Hydraulic Borehole Pressure Cells. Paper in Proceedings of the 28th U.S. Symposium on Rock Mechanics. Univ. AZ, Tucson, AZ, 1987, pp. 273-281.

34. ____. Complete Geomechanical Characterization of Rock Mass With Hydraulic Borehole Pressure Cells. Paper in Proceedings of 29th U.S. Symposium on Rock Mechanics. Univ. MN, Minneapolis, MN, 1988, pp. 725-728.

35. U.S. Bureau of Mines. In Situ Measurement of Rock Stress With Hydraulic Borehole Pressure Cells. Technol. News, No. 316, 1988, 2 pp.

APPENDIX.—SYMBOLS

a	borehole radius
A_1, A_2, A_3, A_4	areas, integrals, of respective stress-distance curves
A_x	Percentage of pillar mined
C	factor for determining in situ deformation modulus
C_s	cell and system stiffness from expansion tests
d	distance
E	elastic modulus of rock
E/R	ratio applicable to a specific calibration cylinder
E_r	rock mass deformation modulus (secant)
G	modulus of rigidity
g	pressure change caused by mining
K	cell response ratio
k_1	constant related to fluid volume retained in CPC
k_2	constant related to response ratio between input and output of CPC pressure
L	CPC length
m	slope of laboratory-derived equations relating pressure cell and rock pressure changes to cell setting pressures
N_1, N_2	premining ground stresses
$N_{1\text{-}0}$, $N_{2\text{-}0}$	biaxial stresses at equilibrium
N_h, N_v	mining-induced horizontal and vertical stresses
p	fluid pressure
p_1, p_2	PCM pressures along calibration curves
P_{bph}, P_{bpv}	horizontal and vertical BPC readings
P_c	fluid pressure change in CPC for each turn of PCM piston
P_{cpc}	CPC pressure reading
$P_{e\text{-}bph}$, $P_{e\text{-}bpv}$	horizontal and vertical BPC equilibrium pressures
$P_{e\text{-}cpc}$	CPC equilibrium pressure
P_i	pressure on inner wall of borehole or cylinder
Q	ratio of horizontal and vertical BPC equilibrium pressures
r	radial distance from pressure cell to borehole wall element
r_i	inside radius of CPC calibration cylinder
S	vertical stress
S_c	geometric factor of BPC (0.185)
S_h, S_v	horizontal and vertical rock stress changes
T	horizontal stress
$T_3 - T_1$, $T_3 - T_2$	difference in PCM turns (borehole-calibration cylinder) at 1,000 psi
V_c	fluid volume change in CPC for each turn of PCM piston
w	opening width
Z, Z_o	normalized axial stresses
α, β	calibration constants
Δp	change in fluid pressure
ΔP_{cpc}	CPC pressure change
ΔP_v	vertical pillar pressure change
ΔS	vertical stress change

ΔT	horizontal stress change
ΔT_p	turn change measured by PCM
ΔV	volume change resulting from PCM displacement
ΔV_i	volume change of borehole or cylinder
ϵ, ϵ_1, ϵ_2	constants for two calibration cylinders
η, η_1, η_2, η_3	pressure-volume slopes from calibration tests
θ	angle between cell axis and stress components
ν	Poisson's ratio
ν_r	Poisson's ratio of rock (secant)
ξ	volume constant (0.0192 in^3) per PCM piston turn
σ_h, σ_v	horizontal and vertical BPC pressure readings
σ_h^*, σ_v^*	horizontal and vertical BPC setting pressures
σ_i	initial vertical stress
σ_r	radial stress
σ_y	premining stress
σ_θ	tangential stress

☆ U.S. GPO: 1991—511-010/42,019

INT.BU.OF MINES,PGH.,PA 29410